RSC Advances

PAPER

View Article Online
View Journal | View Issue

Cite this: *RSC Adv.*, 2025, **15**, 30829

Boosting biodiesel production from WCO utilizing marble waste powder as precursor for CaO/K_2CO_3 nanocatalyst at low temperature *via* RSM optimization

Abdelmoniem H. Abu-Ghazala,†[a] Hosam H. Abdelhady, †*[a] Muhammad G. Abd El-Moghny, *[a] Bassem B. Saied,[a] Anas H. Sayed,[a] Shaymaa T. Kenawy,[a] Omar H. Khalifa,[a] Mhamed A. Rwash[a] and Mohamed S. El-Deab *[ab]

This study aims to valorize hazardous industrial marble machining and shaping waste powder as a precursor to prepare a heterogeneous nano-catalyst (CaO/K_2CO_3) employing the wet-impregnation method for producing biodiesel *via* the transesterification of waste cooking oil (WCO). Surface and morphological characterization of the thus-prepared nano-catalyst has been performed employing various analytical tools, *e.g.*, XRD, BET, CO_2-TPD, FT-IR, HR-TEM, and FE-SEM & mapping EDX. The impact of calcination treatment on the catalytic performance is investigated together with the weight percentage (wt%) of CaO compared to K_2CO_3. Response surface methodology (RSM) is used to optimize the parametric independent variables, *e.g.*, catalyst loading level, reaction temperature, and time, as well as methanol to WCO molar ratio (M : WCO) *via* the central composite design (CCD). The experimentally attained optimal reaction parameters for effective biodiesel production (92%) are: 3.2 wt% catalyst loading, operating at 40 °C for 84 min, along with a 5.8 : 1 M : WCO. The proposed nano-catalyst has been recovered and reused effectively for 5 consecutive cycles, with a slight loss in catalytic activity beginning from the 3rd cycle. Additionally, the quality of the obtained biodiesel perfectly fits the American (ASTM D-6751) and the European (EN-14214) standard limits.

Received 8th July 2025
Accepted 19th August 2025

DOI: 10.1039/d5ra04881h

rsc.li/rsc-advances

1. Introduction

In response to the world's population growth, urbanization, economic expansion, and the advanced industrial revolution, fossil fuel use is steadily increasing to fulfill the rising energy demand.[1–4] Accordingly, the request for securing suitable and viable alternatives for fossil fuels is a must, not only for economic development but also to mitigate the negative environmental drawbacks of utilizing fossil fuels.[5–8] Biodiesel is regarded as the most appropriate and useful renewable liquid biofuel owing to its unique characteristics, *e.g.*, transport simplicity, biological degradability, non-toxicity, and minimal sulphur dosage.[9,10] Biodiesel is an extended fatty acid methyl ester (FAME) chain that is synthesized chemically through the transesterification of triglycerides (edible oil, *e.g.*, sunflower,[11] olive oil[12] *etc.*, and non-edible oil[13,14] *e.g.*, *Cerbera odollam*,[15] or animal fats,[16] *etc.*) with methanol. Whereas FAME is produced along with glycerol as a desirable side product, Fig. 1.[17] Glycerol can be used in a variety of applications, including electro-oxidation of glycerol[18–20] and/or substituting the electro-oxidation reaction in water electrolysis.[21]

Given the prevailing discussion of the energy *versus* food nexus, it is more suitable to utilize waste cooking oil (WCO) for producing biodiesel,[23] which also helps in reducing the manufacturing expenses and reduces waste disposal into the ecosystem, where feedstocks account for approximately 60–75% of the overall expense of the biodiesel commercialization.[24] Catalysts can be categorized as: homogeneous, heterogeneous, and enzyme catalysts. The transesterification process utilizing enzyme catalysts (*i.e.*, *Candida rugosa*, *Oreochromis niloticus*, and *Candida antarctica*[25,26]) produces biodiesel with a high conversion degree under adequate parametric conditions. Despite that, enzyme-based catalysts are relatively expensive with poor tolerance towards stability and reusability. On the other hand, the homogeneous catalysts have high catalytic performance for biodiesel production with high conversion at mild reaction conditions. Heterogeneous catalysts are cheaper and prevail over homogeneous catalysts because of their corrosion resistance, separation simplicity, sustainability, and enhanced lifetime.[13,27–31]

[a]*Department of Chemistry, Faculty of Science, Cairo University, Cairo, Egypt. E-mail: hosamhasan88@cu.edu.eg; gmohamd@sci.cu.edu.eg; msaada@cu.edu.eg; msaada68@yahoo.com*

[b]*Department of Chemistry, Faculty of Basic Science, Galala University, Galala City, 43511, Suez, Egypt*

† Equal first authorship contribution.

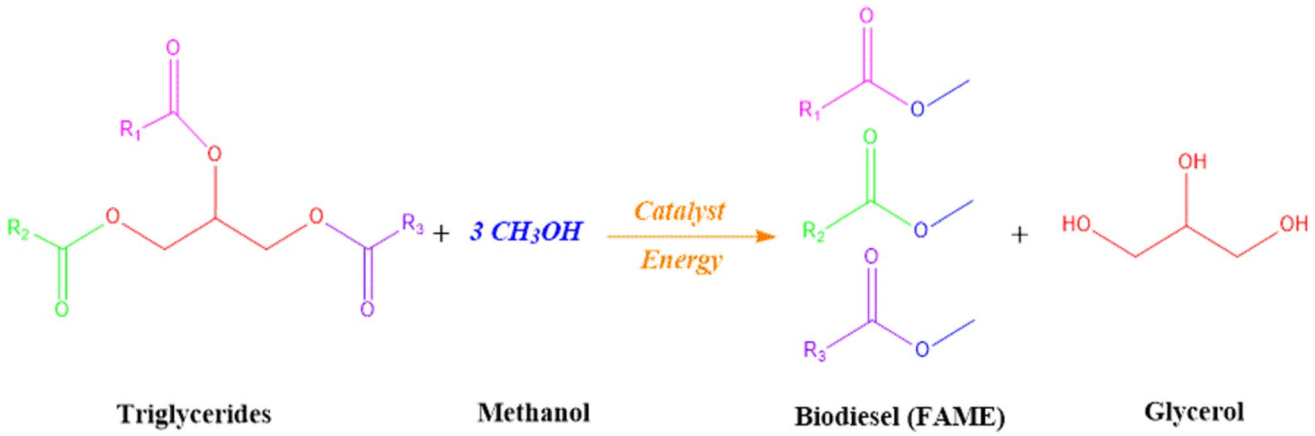

Fig. 1 The chemical equation representing the overall transesterification reaction of TG to biodiesel (FAME).[22]

Alkaline earth metallic oxides (CaO, MgO, SrO, *etc.*) are among the most promising heterogeneous catalyst candidates that can be secured from agricultural and industrial residues.[32,33] This strategy is not only successful in lowering the cost of producing biodiesel fuel but also a prosperous approach for recycling this particular kind of hazardous waste. These pollutants include sugar beet agro-industrial waste,[34] chicken eggshells,[35] white brick waste powder,[22] lime mud from paper waste,[36] and animal bones.[27] Furthermore, K_2CO_3, KF, and KI are diverse, heterogeneous basic catalysts with high catalytic activity in biodiesel production.[37] Among solid base catalysts, K_2CO_3 has demonstrated remarkable activity in methanolysis reactions under mild reaction conditions. However, despite its inherent catalytic potential, the practical application of K_2CO_3 is often limited by its low surface area, limited thermal stability, and poor reusability, which hinder its performance in continuous and large-scale biodiesel production processes. To address these challenges, we have developed a modified nano-catalyst with highly uniform distribution by supporting K_2CO_3 on CaO derived from marble waste powder (MWP). This modification significantly enhances the dispersion, thermal stability, and reusability of K_2CO_3, thereby improving its overall catalytic efficiency. Furthermore, the use of CaO derived from MWP introduces an environmentally friendly aspect by valorizing industrial by-products, aligning the catalyst design with principles of green chemistry and sustainable development. In previous studies, various heterogeneous K_2CO_3-based catalysts have been used to produce biodiesel, including K_2CO_3/$MgFe_2O_4$,[38] CaO–$MgFe_2O_4$/K_2CO_3,[39] CuO/K_2CO_3,[40] K_2CO_3/γ-Al_2O_3.[41]

Several variables affect the transesterification process, including the catalyst loading, reaction temperature and time, methanol to WCO molar ratio (M : WCO), and agitation speed. For commercialization purposes, these reaction factors must be optimized to lower the expense of the biodiesel manufacturing methodology.[41] Response surface methodology (RSM) is a quantitative and statistical concept that is funded on several design methodologies such as Central Composite Design (CCD), Optimal (Custom) Design, Definitive Screen Design (DSD), and Box–Behnken Design (BBD) that is employed to refine and optimize the reaction parameters and determine the influence of independent variables on the reaction procedure.[42,43] From this methodology, "biodiesel conversion" is defined as the dependent variable. Whereas the reaction time and temperature, M : WCO, and catalyst loading are considered independent variables, which all influence the biodiesel conversion efficacy.[44]

This study introduces a novel and sustainable approach by converting marble waste powder (MWP) into a low-cost CaO-based nano-catalyst for biodiesel production from waste cooking oil (WCO) under mild conditions. This method addresses key environmental issues associated with MWP and WCO disposal while enhancing the efficiency of the transesterification process. This study advances sustainable biofuel technologies by valorizing industrial and household waste streams. In doing so, it aligns with circular economy principles by promoting the recovery of resources and the conversion of waste into valuable energy products. The surface and morphological characterization of the CaO/K_2CO_3 nano-catalyst is conducted based on diverse tools, *e.g.*, X-ray diffraction (XRD), nitrogen adsorption–desorption isotherm, Fourier transform infrared spectroscopy (FT-IR), CO_2-temperature programmed desorption (CO_2-TPD), and scanning electron microscope (SEM) with mapping EDX. RSM, based on the CCD statistical approach, is employed to get the optimal reaction conditions for the methanolysis process to accomplish the optimum biodiesel conversion. In order to maximize the economic benefit of the proposed nano-catalyst, the reusability of the proposed nano-catalyst is also considered. Furthermore, the applicability of the FAME in vehicles is inspected by studying the fuel quality and matching with the international limits of ASTM D-6751 and EN-14214.

2. Materials and methods

2.1. Chemicals and materials

The utilized WCO (residue from the frying food industry) was purchased from Tagaddod Egypt Co. (6th of October City,

Egypt). The physical properties of the used WCO are reported in Table 1, and the fatty acid profile is shown in Table S1. MWP was obtained from a local marble processing facility (Shaq EL-thoban district, Cairo, Egypt). Sigma-Aldrich supplied methanol (99.5%), while Löba Chemie provided the potassium carbonate tetrahydrate ($K_2CO_3 \cdot 4H_2O$). Panreac Qümica supplied the deuterated chloroform ($CDCl_3$).

2.2. Nano-catalyst preparation

MWP was sieved into small sizes and ground into powder to get the highest potential surface area. Subsequently, MWP had to be calcined inside a muffle furnace at 800 °C for 3 h with a heating rate of 20 °C min^{-1} to prepare CaO. Then, the product was maintained in a desiccator.

CaO/K_2CO_3 was synthesized *via* a wet impregnation method. A predetermined amount of K_2CO_3 was dissolved in 100 mL of deionized water, yielding a naturally alkaline solution (pH ∼ 10.5). The required amount of calcined MWP (CaO) was then gradually added under continuous stirring to ensure homogeneous dispersion and interaction between the components. The obtained mixture was thoroughly aged for 2 h with continuous magnetic stirring at 700 rpm, then extra water was removed *via* evaporation at 80 °C and was entirely dried in a drying oven at 100 °C overnight. The leftover solid particles were calcined at 500 °C (heating rate of 20 °C min^{-1}) for 2 h.

2.3. Catalyst characterization

The crystallographic composition of the CaO/K_2CO_3 nano-catalyst was determined through the Bruker-XRD (D8 Discovery Diffractometer Device-Bruker XRD, Karlsruhe, Germany) applying an X-ray cylinder alongside radiation of Cu K_α (λ = 1.5418 Å), with a cylinder voltage of 50 kV and an applied current of 20 mA over a 2θ (10–80°) angle region. The functional groups of the proposed nano-catalyst were identified through FT-IR spectroscopy (Agilent Technology Version Cary 630-Agilent Technologies, California, USA) using a spectrum band of 400 to 4000 cm^{-1}. The nanoscale morphology of the as-prepared nano-catalyst has been demonstrated by applying high-resolution transmission electron microscopy (JEM-HR-JEOL-JEM 2100-JEOL Ltd, Tokyo, Japan), revealing insight into the atomic structure of the substance from the acquired pictures. Field emission scanning electron microscopy (FE-SEM, QUANTA FEG 250) was used to demonstrate the surface's microstructure, operated at 10.0 kV accelerating voltage with a 19 mm working distance using a secondary electron detector; images were acquired at 5000× magnification under high vacuum mode. Before imaging, the samples were sputter-coated with a thin layer of gold to enhance conductivity and image quality.

The precise surface area of the derived sample was appraised employing the Brunauer–Emmett–Teller (BET) approach on a volumetric adsorption instrument at −196 °C by studying the N_2-adsorption/desorption isotherm (surface area & pore size analysis [Belsorp III, Japan]). The fundamental basic character of the calcined nano-catalyst (CaO/K_2CO_3) surface was investigated through CO_2-temperature-programmed desorption (TPD) [BEL-Cat, Japan]. To eliminate any adsorbed stacking species from the sample surface, it was subjected to heating at 200 °C for 30 min under helium injection. The sample was then inflated with 5% CO_2 and helium at a rate of 20 mL min^{-1} for 30 min.

Table 1 The physicochemical characteristics of the used WCO

Physicochemical characteristics	Units	Value
Density	g cm^{-1}	0.92
Free fatty acid (FFA)	%	0.7
Kinematic viscosity	mm^2 s^{-1}	38
Iodine value	g I_2 per 100 g oil	138.7
Acid value	mg KOH per g	1.4
Water content	%	<1%
Peroxide number	meq. per kg	27.1

2.4. Transesterification methodology

The methanolysis reaction of WCO into biodiesel (also referred to fatty acid methyl ester, FAME) was carried out in open air using a triple-necked bottom glass flask, submerged in a heating oil bath on a hot plate with a stirring magnet connected to a temperature probe immersed in the system mixture, attached with a water-cooled condensing apparatus. The WCO was added to the flask and then pre-heated for 20 min to the required temperature (40 °C) before the injection of CaO/K_2CO_3 nano-catalyst and methanol mixture. To ensure the symmetry and elimination of mass transfer restrictions, the reaction was left to run for the allotted period while being continuously stirred at a constant agitation speed of 700 rpm. To determine the best conditions for the conversion process, several sets of reactions were implemented at a reaction temperature of 40 °C with various parameters, *e.g.*, catalyst loading (2–5%), methanol-to-WCO ratio (5 : 1–9 : 1), and reaction duration (60–180 min).

The catalyst and biodiesel mixture were separated after the allotted reaction time by centrifuging (EBA 200 model – Hettich, Germany) for 10 min at 6000 rpm. The catalyst was in the bottom layer, while the biodiesel-containing glycerin was in the top layer. Glycerol and biodiesel were separated *via* a separatory funnel, with glycerol (the heavier component) at the bottom and biodiesel residing in the upper layer. Moreover, the extra methanol (unreacted) was recovered by simple distillation. This recovery method is an essential part of a cost-effective and sustainable biodiesel production. The attained biodiesel was then repeatedly rinsed in hot distilled H_2O to detach the catalyst and glycerol residues, as shown in Fig. 2.

2.5. Product quantification

Proton nuclear magnetic resonance (^{1}H-NMR) spectral data (obtained by Mercury Varian (VX-300) NMR, operating at 300 MHz) were used to quantitatively examine the biodiesel conversion from the WCO through the transesterification process as per eqn (1). $CDCl_3$ was the solvent used in ^{1}H-NMR analysis (see Fig. S1).[45]

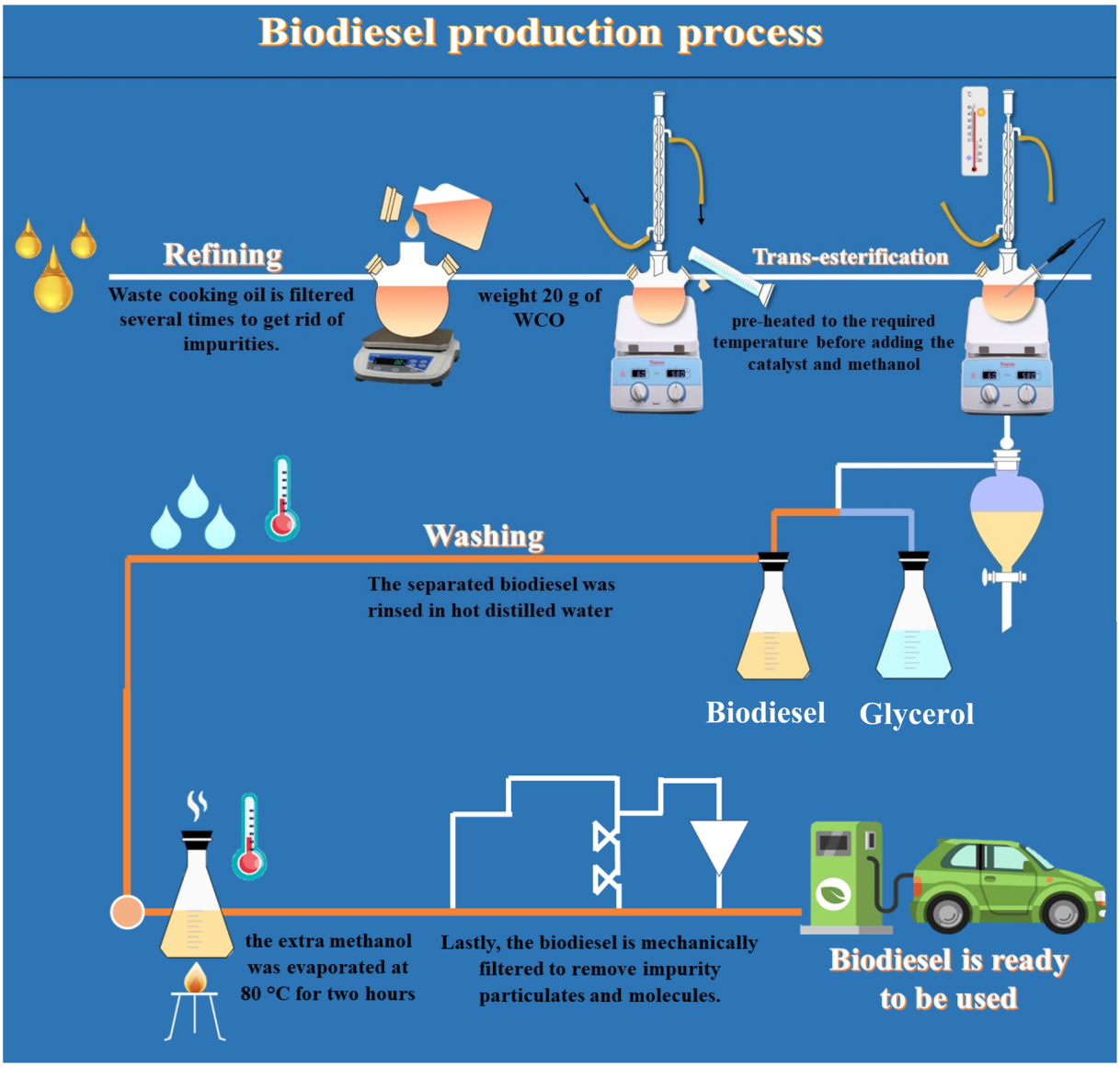

Fig. 2 Graphical representation of the biodiesel production approach used in the current study.

$$\text{Conversion } (\%) = \frac{2 \times A_{\text{O–CH}_3}}{3 \times A_{\alpha\text{-CH}_2}} \times 100 \quad (1)$$

where $A_{\text{O–CH}_3}$ represents the peak integration for the methyl esters that appeared at 3.66 ppm, and $A_{\alpha\text{-CH}_2}$ reflects the peak integration for the methylene, which was detected at 2.28 ppm.

2.6. Response surface methodology (RSM)

The RSM is a series of statistics and applied mathematics methodologies for progressing experimental simulations that are used for optimizing the reaction variable parameters and spotting the influence of both dependent and independent factors on the methanolysis reaction. The object of such an approach is to indicate the response pattern and to identify the parametric optimal conditions of biodiesel production variables through a methanolysis reaction of WCO. Design-Expert software® version 13.0.5 is based on the design of the experiment (DOE), RSM, and applying CCD was employed to adjust the various conditions of the biodiesel transesterification methodology. This approach includes a pre-optimization stage, which requires numerous experimental runs to evaluate the conditions' margins toward the ideal biodiesel conversion. In this study, the 4-level 3 factors mode of a CCD was applied to optimize the three independent factors of catalyst loading level (A), M : WCO (B), and reaction time (C). The CCD-independent

Table 2 Margins of the three transesterification individual variables: (A) catalyst loading, (B) M : WCO, and (C) time applied in RSM design

Factors (Unit)	Min.	Max.	$-\alpha$	$+\alpha$
Catalyst loading (%)	2.61	4.39	2	5
M : WCO	5.81	8.18	5	9
Time (min)	84.3	155.7	60	180

margins for adjusting the reaction factors for the methanolysis reaction are displayed in Table 2. Corresponding to eqn (2), N is the number of experimental runs, n is the factors number and m expresses the center points. Accordingly, there are 8 factorial points, 6 axial points, and 6 replicated center points. As indicated in Table 3, 20 experimental runs were carried out in a randomized sequence as calculated from eqn (2). Note that the experimental runs are carried out at a constant temperature of 40 °C. Thus, it is not indicated as a variable in this investigation.

$$N = 2^n + 2n + m = 2^3 + 2 \times 3 + 6 = 20 \text{ runs (where } n = 3) \quad (2)$$

Analysis of variance (ANOVA) was implemented in this approach to analyze the experimental data and identify the coefficient values of the consequent polynomial simulation. The determination coefficient (R^2) was estimated to assess the statistical significance of the polynomial system's output, and the f-value and p-value were determined to evaluate its accuracy. RSM design was employed to estimate the experimental data according to the quadratic polynomial model as shown in eqn (3).

$$Y = b_0 + \sum_{i=1}^{k} b_i x_i + \sum_{i=1}^{k} b_{ii} x_i^2 + \sum_{i_{i>j}}^{k} \sum_{j}^{k} b_{ij} x_i x_j + e \quad (3)$$

where k signifies the summation of variables that were investigated and optimized, while e shows the variance of the experiment assigned to the dependent factors Y, b_0 indicates the intersection point, b_i represents the first-order factor, X_i is the ith independent parameter, b_{ii} signifies a quadratic factor for X_i, b_{ij} expresses the coefficient of linearity for the effect of the interaction of the ith and jth parameter, and Y is the coefficient of response (biodiesel conversion%).

2.7. Catalyst lifetime

The catalyst lifetime assessment was conducted within the optimal transesterification conditions for 5 consecutive cycles, employing the same catalyst concentration each time, to assess the reusability of the catalyst. After each cycle, the catalyst was centrifuged to be detached and then washed with methanol to get rid of the residual oil and glycerol. The catalyst was then dried at 80 °C for 4 h. The catalyst was then recalcined at 900 °C for 3 h with a heating rate of 20 °C min^{-1} to reactivate the catalyst's active sites.

3. Results and discussion

3.1. Characterization of the nano-catalyst

XRD, BET surface area, CO_2-TPD, FT-IR, HR-TEM, and FE-SEM & EDX are among the techniques employed for identifying the morphological and surface characterizations of MWP and the as-prepared nano-catalyst (CaO/K_2CO_3).

3.1.1. XRD analysis. The XRD structure patterns for the synthesized nano-catalyst are studied, as shown in Fig. 3. The diffraction spectrum of the calcined MWP at 800 °C (M-800) shows peaks appeared at 2θ = 32.2°, 37.3°, 53.9°, 64.1°, and 67.5°, which are corresponding to (1 1 1), (2 0 0), (2 2 0), (3 1 1), and (2 2 2) facets, respectively, and match nicely with the conventional JCPDS reference card: (00-037-1497) as depicted in Fig. 3a. These diffraction patterns constitute the crystalline phase of CaO. Whereas the diffraction peaks at 2θ = 27.8°, 34.2°, and 41.1° with the standard JCPDS reference card: (01-084-1270), are assigned to the physical adsorption of H_2O

Table 3 RSM design result matrix of the dependent (expected FAME conversion%) and independent variable (response parameters) (depending on the CCD)

Run	Variable catalyst loading (wt%)	Variable M : WCO	Variable time (min)	Conversion (%)		Residual
				Experimentally verified	Model prediction	
1	3.5	7	120	95.73	95.72	0.01
2	4.39	8.19	155.7	93.08	94.02	−0.94
3	2.61	5.81	155.7	93.64	93.01	0.63
4	4.39	5.81	84.3	97.75	97.71	0.04
5	2.61	8.19	155.7	91.79	91.71	0.08
6	4.39	5.81	155.7	98.03	98.47	−0.44
7	5	7	120	97.05	95.90	1.15
8	3.5	9	120	99	98.47	0.53
9	3.5	7	120	95.73	95.72	0.01
10	2.61	8.19	84.3	90.86	90.29	0.57
11	3.5	7	120	95.73	95.72	0.01
12	4.39	8.19	84.3	100	100.50	−0.50
13	3.5	7	120	95.73	95.72	0.01
14	3.5	7	180	95.83	95.37	0.46
15	3.5	5	120	96.51	97.22	−0.71
16	3.5	7	120	95.73	95.72	0.01
17	3.5	7	120	95.73	95.72	0.01
18	3.5	7	60	92.9	93.54	−0.64
19	2.61	5.81	84.3	85.42	84.36	1.06
20	2	7	120	81.4	82.73	−1.33

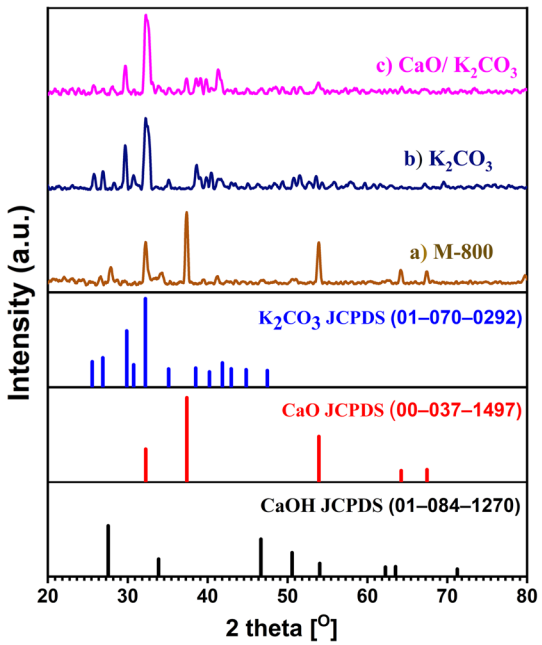

Fig. 3 XRD patterns for (a) calcined MWP (M-800), (b) utilized K_2CO_3 for catalyst preparation, and (c) the as-synthesized nano-catalyst CaO/K_2CO_3.

molecules on the CaO surface as a result of the calcined sample being directly exposed to ambient air during the measurement procedure, forming $Ca(OH)_2$.[22] The spectral pattern of K_2CO_3 utilized for the catalyst's synthesis peaked at 25.7°, 26.9°, 29.9°, 30.7°, 32.2°, 35.1°, 38.5°, 40.4°, 51.5°, and 53.5°, with the JCPDS standard reference card: (01-070-0292), which correlate to the crystalline structure of the high crystallinity of K_2CO_3 phase (see Fig. 3b). The XRD diffraction pattern of the proposed nano-catalyst CaO/K_2CO_3, as depicted in Fig. 3c, shows a hybrid pattern of both CaO and K_2CO_3, which is considered an indication of the highly uniform distribution of the proposed nanocatalyst, which might be reflected in its catalytic efficacy in the methanolysis process.

The average particle size (D_p) of CaO and CaO/K_2CO_3 is determined by applying the widely utilized Debye–Scherrer equation, which is given in eqn (4) and is based on the intensity value of the highest intensity peak in the XRD pattern.[46]

$$D_p = \frac{\lambda}{\beta \cos \theta} \quad (4)$$

where D_p denotes the mean crystalline size, K' denotes the crystalline aspect ($K' = 0.9$), λ signifies the wavelength of X-ray radiation for Cu K_α, β is the pattern's full width at half maximum (FWHM), and θ expresses the diffraction angle for the (h k l) peak or Bragg's angle. The average crystalline size of CaO (M-800), K_2CO_3, and CaO/K_2CO_3 was 20.5, 18.3, and 14.6 nm, respectively, implying nano-scale material synthesis as listed in Table 4.

3.1.2. FT-IR analysis. FT-IR spectra for calcined M-800, K_2CO_3 used in catalyst synthesis, and the as-synthesized CaO/K_2CO_3 nano-catalyst, as per in Fig. 4. The absorption peaks of

Table 4 Crystalline size for the calcined MWP (M-800), K_2CO_3, and the as-synthesis CaO/K_2CO_3 nano-catalyst

Catalyst	Crystalline size[a] (nm)	FAME conversion[b] (%)
CaO (M-800)	20.5	50.9
K_2CO_3	18.3	58.6
CaO/K_2CO_3	14.6	100

[a] Based on the XRD pattern through the origin (version b-9.5.0.193). [b] Biodiesel conversion (%) calculated using ^{1}H-NMR after the transesterification reaction carried out using M : WCO of 9 : 1, catalyst loading of 5 wt% operated at 60 °C for 120 min.

M-800, as shown in Fig. 4a, appear at wavenumbers of 900 and 1024 cm^{-1}, which can be assigned to the carbonate (CO_3^{2-}) group's asymmetric stretching, out-of-plane, and in-plane vibration.[22] Ca–O stretching vibration is also exhibited in the absorption bands at 433 and 522 cm^{-1}. Furthermore, the absorption band at 3668 cm^{-1} might be attributed to surface hydroxyl (–OH) stretching vibration. That's owing to adsorbed water molecules from the air within the sample measurement, caused by the hygroscopic characteristics of CaO. The absorption bands of K_2CO_3 are located at 1430, 1390, 887, and 713 cm^{-1}, which can be attributed to the CO_3^{2-}. The as-prepared nanocatalyst CaO/K_2CO_3 exhibits hybrid absorption bands corresponding to the (CO_3^{2-}) stretching peak (*i.e.*, at wavenumbers 1412 and 822 cm^{-1}) and the Ca–O stretching vibration band (*i.e.*, at wavenumber 528 cm^{-1}). This confirms the homogeneous uniform distribution of CaO with K_2CO_3, which is consistence with the XRD patterns shown in Fig. 3.

3.1.3. XRF analysis. X-ray fluorescence (XRF) analysis was performed to determine the elemental composition of MWP, and the results are presented in Table S2. The analysis revealed that CaO is the dominant component, accounting for 94.24 wt%, confirming the highly basic nature of MWP. Minor quantities of other basic oxides, such as MgO, Na_2O, and K_2O,

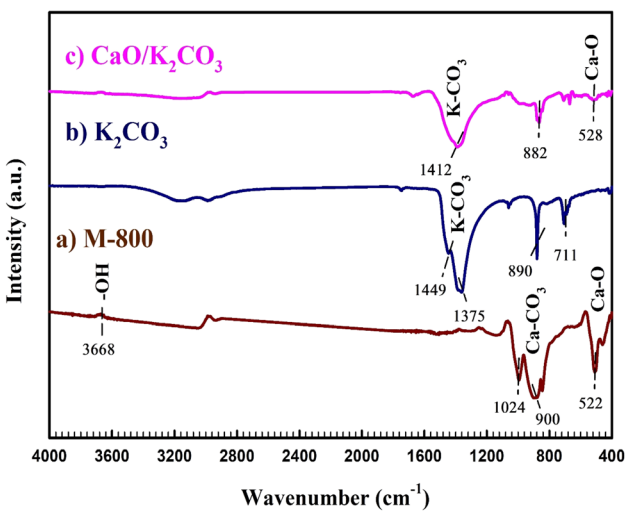

Fig. 4 FT-IR spectroscopy for (a) calcined MWP (M-800), (b) utilized K_2CO_3 for catalyst preparation, and (c) the as-synthesized nano-catalyst CaO/K_2CO_3.

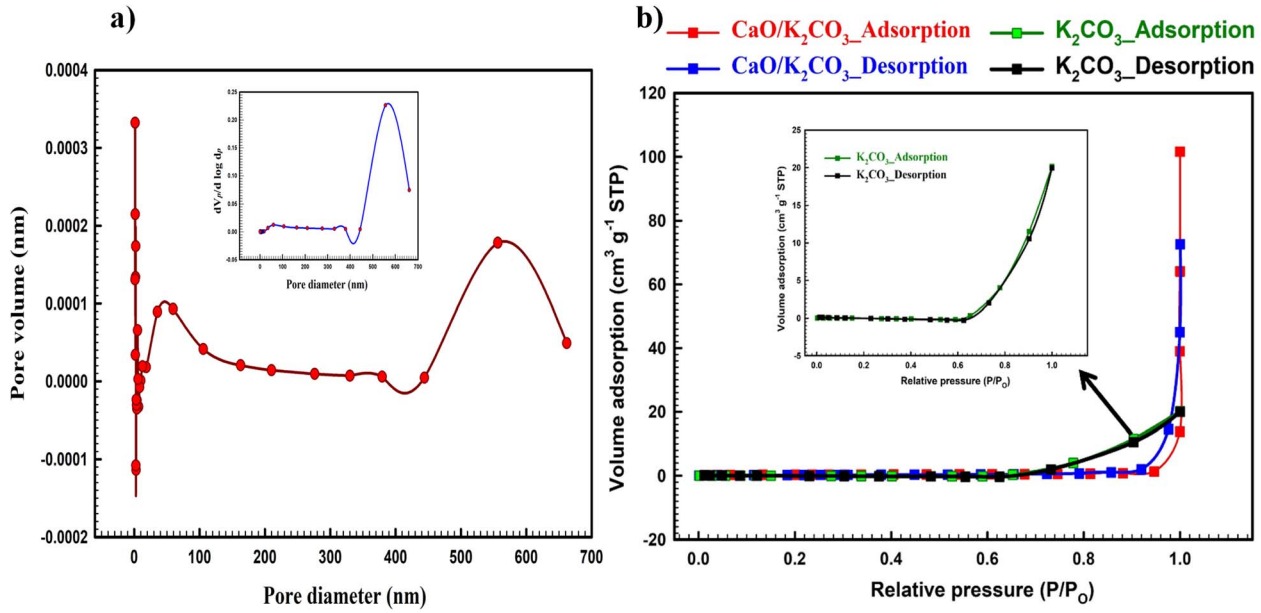

Fig. 5 (a) BET–BJH analysis and pore volume distribution of CaO/K_2CO_3 (inset of the distribution of pore size for the prepared CaO/K_2CO_3), and (b) BET-N_2 adsorption–desorption isotherm of the as-prepared CaO/K_2CO_3 and K_2CO_3 (inset).

were also detected, along with small amounts of amphoteric (Al_2O_3) and acidic oxides (SiO_3 and P_2O_5). The presence of both basic and acidic metal oxides suggests potential catalytic activity in transesterification and esterification reactions, enhancing the material's suitability as a heterogeneous catalyst.

3.1.4. BET isotherm analysis. In order to produce biodiesel, triglyceride (TG) molecules must come into contact with the basic sites on the outermost layer of the catalyst or within the catalyst's porosity. Pores must be sufficient to allow entry of TG molecules, with sizes ranging from 3–6 nm, to the basic active sites.[47,48] As a result, BET–BJH isotherm information, as shown in Fig. 5a, is critical for comprehending the catalysts' capacity to diffuse big molecules of TG into catalyst pores and access basic sites within pores.[49] Fig. 5b depicts the N_2 adsorption–desorption of the as-synthesized nano-catalyst (CaO/K_2CO_3). The catalyst exhibited predominantly macroporous characteristics based on the average pore diameter. CaO/K_2CO_3 had a specific surface area of 1.35 $m^2\ g^{-1}$, a mesopore volume of 0.31 $cm^3\ g^{-1}$, and an average pore diameter of 53.01 nm, based on BET measurement. Furthermore, heat treatment inspired the perforations to be dispersed non-uniformly and broadly. Catalysts with a broad hole distribution work superior in the FAME production. It is worth mentioning here that the surface area of pristine K_2CO_3 (Fig. 5b) is 0.06 $m^2\ g^{-1}$. The low surface area of pristine K_2CO_3 is due to the crystalline nature of the material, and/or it has a closed pore structure.

3.1.5. FE-SEM and mapping EDX analysis. The surface structure of the calcined MWP (M-800) and the prepared nano-catalyst (CaO/K_2CO_3) was compared with FE-SEM and coloured mapping EDX analysis, as per in Fig. 6(a and b). According to the FE-SEM data, M-800 has a cluster morphology and a spongy framework, with particles shaped into clusters, indicating oxide formation is due to the elevated temperature throughout the calcination of MWP, as exhibited in Fig. 6. This reduced particle size correlates with the specific surface area calculated using BET isotherms. In contrast, the CaO/K_2CO_3 exhibits nano-aggregation of needles, indicating a uniform homogeneous distribution of K_2CO_3 into the porous oxide of M-800, as shown in Fig. 6.

The EDX analysis depicts a uniform expansion of species in the sample data. The EDX-mapping analysis of M-800 with Ca (46.4%), O (48.6%), and C (5.0%) shows that raw MWP is composed mainly of $CaCO_3$, which is decomposed during the calcination process, resulting in CaO with CO_2 evolution. The EDX of the as-synthesized CaO/K_2CO_3 nano-catalyst reveals Ca (7.62%), O (47.3%), C (10.2%), and K (34.9%), as shown in Fig. 6, which discloses the good distribution of both K_2CO_3 and CaO.

3.1.6. HR-TEM analysis. HR-TEM is a powerful technique revealing the atomic morphology of the fabricated CaO/K_2CO_3 nano-catalyst as shown in Fig. 7. The prepared nano-catalyst morphology modelling displays a porous configuration resembling a sponge's interior and entanglement-created nanometric cracks. A statistical approach is employed to determine the catalyst's nanoparticle size distribution, as shown in Fig. 7c, which has an average dimension of 22.8 nm. The substantial surface area of the prepared CaO/K_2CO_3 is a result of this morphological modification. The uniform distribution of CaO/K_2CO_3 inspected from TEM photos, supports a steady nano-frame for the CaO particles, which deeply enriches the catalytic activity of the as-synthesized catalyst. The selected area electron diffraction (SAED) pattern is shown in Fig. 7d. SAED exhibits extremely small bright spots wrapped by a ring-like diffraction electron sequence, validating the crystalline structure of the CaO/K_2CO_3 nanocatalyst.

3.1.7. CO_2-TPD analysis. The CO_2-TPD technique is applied to study the basicity of the synthesized catalyst, which reflects

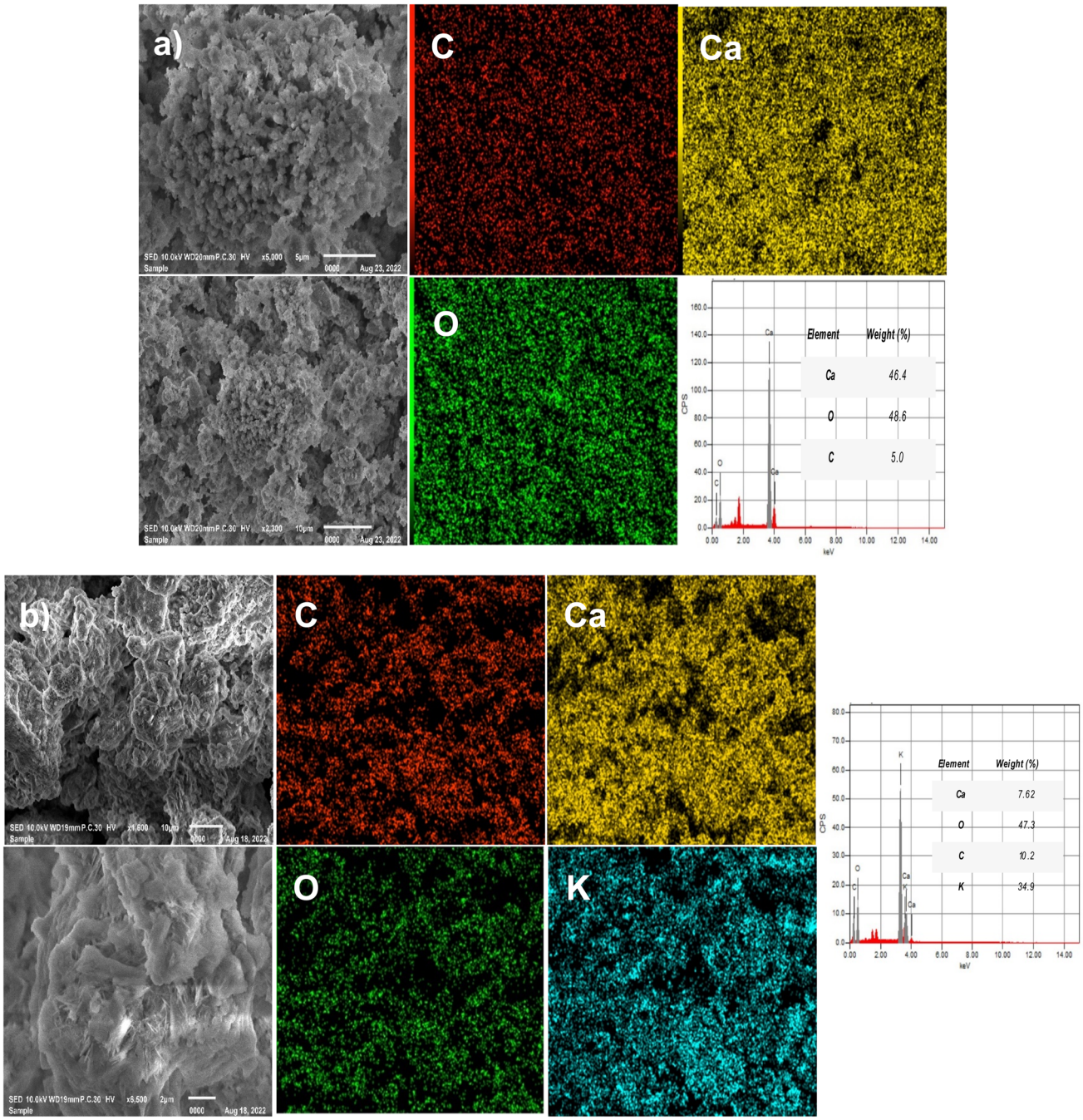

Fig. 6 FE-SEM and mapping EDX of (a) calcined MWP (M-800), and (b) prepared CaO/K_2CO_3 nano-catalyst.

the catalytic performance in the transesterification reaction.[41,50] The quantity of CO_2 particles adsorbed on the exterior layer of the catalyst, which corresponds precisely to the catalyst's basic active sites, is used for measuring the catalyst's basicity. The CO_2-TPD graph fundamentally rationalizes three separate zones. The first crest correlates with the weak basic desorption sites at <200 °C. At temperatures ranging from 200 to 450 °C, the second area predicts modest basic active sites for CO_2 desorption. As a result, the CO_2-temperature basic desorption region is located at temp. >450 °C indicates the presence of robust basicity due to a strong interaction among the adsorbed molecules of CO_2 and catalyst basicity. Subsequently, the basicity of the catalyst can be anticipated by integrating the region of the corresponding basic desorption bands.[51]

Fig. 8 presents the CO_2-TPD desorption profiles of CaO and CaO/K_2CO_3 catalysts. The CaO/K_2CO_3 sample (red curve) exhibits three distinct desorption peaks centered around 130 °C, 500 °C, and 790 °C, corresponding to weak, moderate, and strong basic sites, respectively. In contrast, the CaO sample (blue curve) shows only a prominent desorption peak at ~790 °C, indicating the presence of primarily strong basic sites. The introduction of K_2CO_3 significantly enhances the basicity of

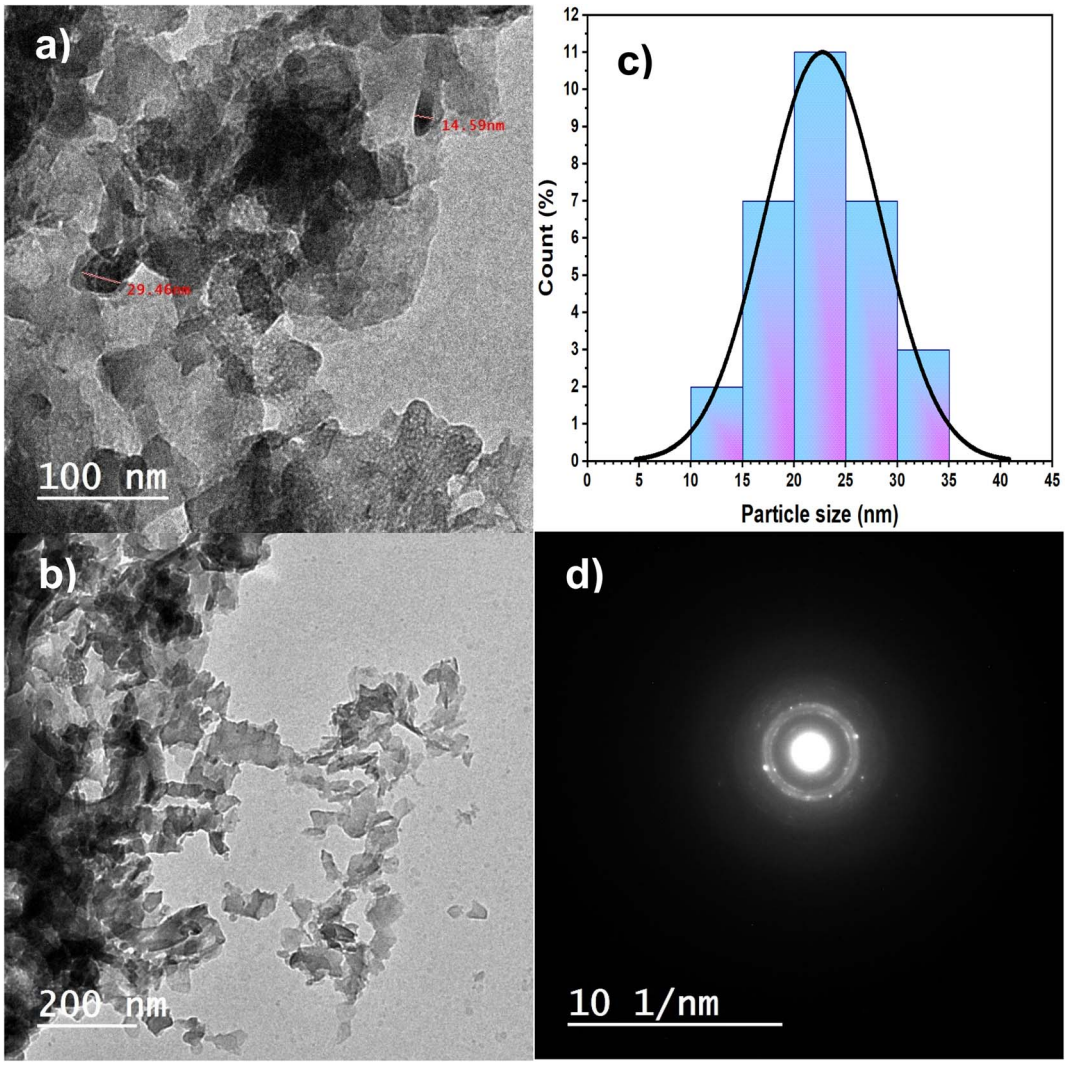

Fig. 7 HR-TEM images at various magnifications (a and b), statistical particle size distribution (c), and SAED pattern (d) of the prepared CaO/K_2CO_3 nanoparticles.

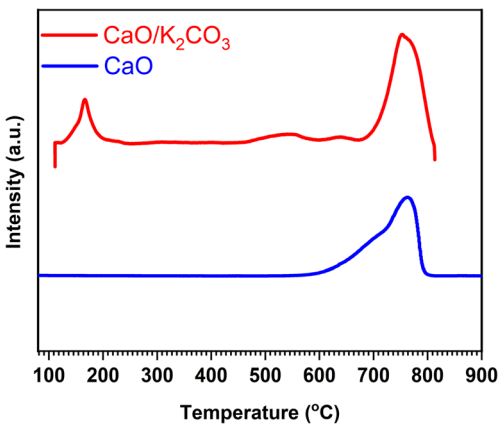

Fig. 8 CO_2-TPD analysis for CaO-derived MWP and CaO/K_2CO_3 nano-catalyst.

CaO by increasing the density and diversity of basic sites. This synergistic effect improves the catalyst's performance in base-catalyzed reactions, such as transesterification, by facilitating easier hydrogen abstraction and methoxide formation under milder conditions.

3.2. Transesterification parameter optimization

3.2.1. Influence of molar ratio CaO/K_2CO_3. The prepared CaO : K_2CO_3 catalyst with different molar ratios (calcined at 600 °C for 2 h) has a marked influence on biodiesel conversion, which can achieve a high conversion rate for producing biodiesel at a relatively low reaction temperature, as shown in Fig. 9. Under reaction conditions of 60 °C for 120 min, M : WCO molar ratio of 9 : 1, and catalyst loading of 5 wt% of MWP without K_2CO_3 (calcined at 600 °C for 3 h) produced a low biodiesel conversion of 50.9%. This is owing to the high reaction temperature necessary to speed up the methanolysis reaction. As a consequence, the main target is to support K_2CO_3 with CaO-based MWP, which is remarkable for its high basicity. Increasing the molar ratio of K_2CO_3 relative to CaO, under the same methanolysis reaction parameters, resulted in a higher biodiesel conversion at a low optimized reaction temperature.

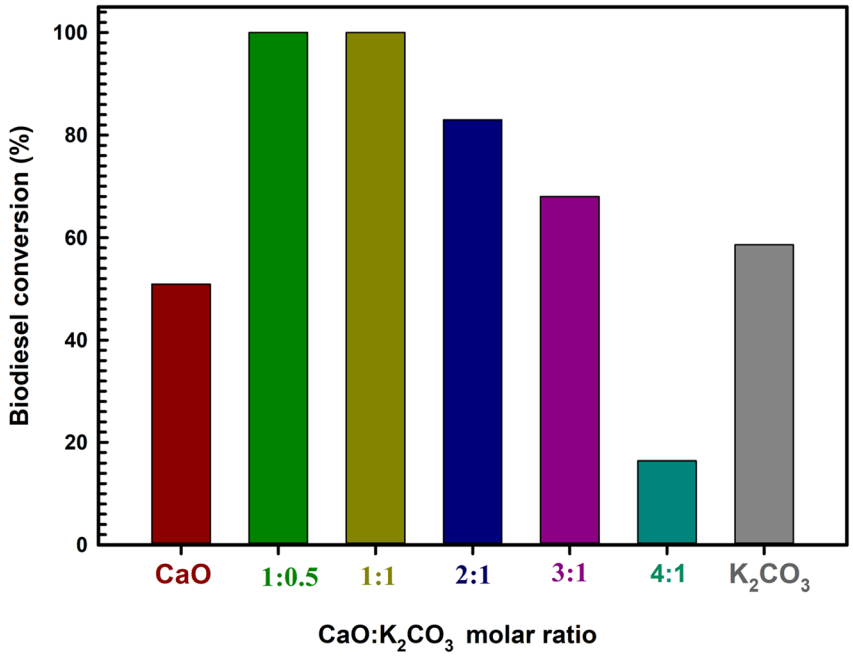

Fig. 9 Optimizing the CaO : K_2CO_3 molar ratio for biodiesel conversion *via* the transesterification process over experimental parameters at 60 °C for 120 min, M : WCO of 9 : 1, and a constant catalyst loading of 5 wt%.

According to Fig. 9, a 4 : 1 molar ratio (CaO : K_2CO_3) achieves the lowest biodiesel conversion of 16.4%. While molar ratios of 3 : 1 and 2 : 1 attain larger biodiesel conversion of 68% and 83%, respectively, than that of only calcined MWP. The molar ratios (1 : 1 and 1 : 2) of CaO : K_2CO_3 result in the maximum biodiesel conversion (*ca.* 100%). Based on this data, the optimal CaO : K_2CO_3 molar ratio is 1 : 1, as it achieves the highest biodiesel conversion with the minimum quantity of K_2CO_3.

3.2.2. Influence of calcination temperature. Calcination temperature has significant consequences on biodiesel conversion as it deeply affects the catalytic performance, as depicted in Fig. 10. The lowest biodiesel conversion (*C*, 28.2%) is achieved at a calcination temperature of 400 °C because it is insufficient for the catalyst activation monitoring. At 500 and 600 °C, biodiesel conversion is expanded to be three times more than the former value (at 400 °C) with an increase in the calcination temperature; calculated biodiesel conversion at these temperatures is 100%. The biodiesel conversion rate has dropped to 96.3% at calcination of 700 °C, which is a lower conversion than that obtained at calcination of 500 and 600 °C. This is due to particle agglomeration and sintering, which reduced the catalyst surface area and hence inhibited the biodiesel conversion.[22] The optimal calcination temperature is 500 °C for 2 h, since this results in a superior biodiesel conversion at the lowest possible calcination temperature.

3.2.3. RSM analysis. The optimization methodology of the transesterification variables, *e.g.*, [*A*] catalyst loading, [*B*] M : WCO [*C*] time, is studied *via* statistical CCD through RSM according to the respective data from 20 experimental runs (see Table 3). The polynomial model is a significant framework for demonstrating the ideal conditions to produce FAME through the methanolysis reaction. Eqn (5) displays the coded equation of parametric variables for the polynomial model of biodiesel conversion (%).

$$\text{Conversion (\%)} = 95.72 + 3.92A + 0.3718B + 0.5446C - 0.7863AB - 1.97AC - 1.81BC - 2.27A^2 + 0.7492B^2 - 0.4493C^2 \quad (5)$$

where factors (*A*, *B*, and *C*) signify the variable parameters of catalyst loading, M : WCO, and time, consecutively. Through the previous formula, the positive variance code has an affirmative

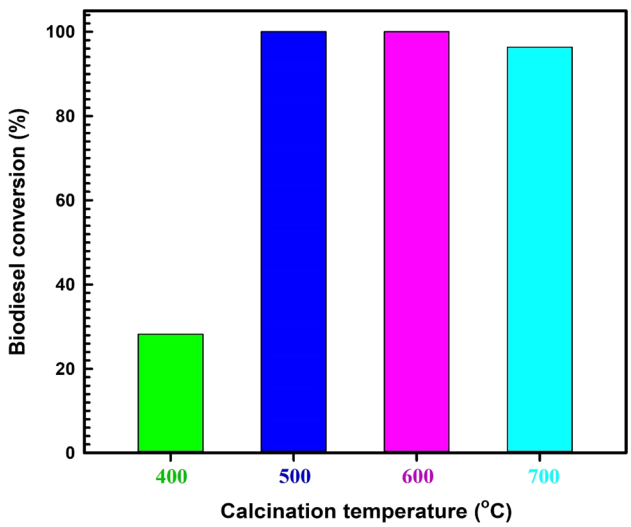

Fig. 10 Calcination temperature influence on biodiesel conversion (400–700 °C) with reaction parametric conditions of 60 °C for 120 min, M : WCO of 9 : 1, and 5 wt% of catalyst loading.

change on the biodiesel conversion (%). Otherwise, the negative variance code indicates an adverse influence on the biodiesel conversion (%). ANOVA is a statistical method to clarify the differences or correlations between independent restrictions (*i.e.*, catalyst loading, M : WCO, and time) and their influence on the dependent parameter (*i.e.*, biodiesel conversion%) according to statistical factors such as multiple determination (R^2), *f*-value, and *p*-value, which are listed in Table 5. The *f*-value for the suggested quadratic polynomial design is 53.13, which implies a high significance of the proposed statistical polynomial design. Otherwise, the *p*-value for the suggested model seems <0.0001 (<0.05), which specifies a highly significant statistical model for the response of the biodiesel manufacturing methodology. This is significantly reflected in the high statistical measurement of multiple determination (R^2), which is 0.9795, while the adjusted R^2 is 0.9611, where R^2 represents the multiple determination experimentally verified result, and adjusted R^2 represents the anticipated result. This validates the theoretical design and the experimental verified results agreement. Fig. 11a depicts a comparison chart for the anticipated and the actual biodiesel conversion; the actual outcomes are uniformly distributed and close to the predicted values (straight line). This illustrates that the established statistical model can accurately describe the correlation between the independent factors and the response parameter (biodiesel conversion%). Because the outcomes are frequently distributed in a straight line, the error within the system's settings is negligible.

The standard probability diagram for residual results (see Fig. 11b) assesses the adequacy of the proposed model corresponding to residuals before completing the optimization methodology, because the residual points remain roughly along a straight line, implying that the residuals comply with the standard distribution. All the response data in the diagram of externally studentized residuals *vs.* response predictions data of the biodiesel manufacture are presented in Fig. 11c, which is assigned indiscriminately to the reference baseline. Overall, the regression model reveals that the biodiesel manufacturing method is quite adequate. The model is stable since all of the expected data fall within the 4% allowed error range. The diagram of externally studentized residuals *vs.* experimental reactions in Fig. 11d reveals that all data points in both techniques drop arbitrarily toward the midline. Few spots receive a larger reaction than others since the residual value is relatively low and presented around the central line.

3.2.4. Model verification and fitting. CCD-based RSM is implemented to illustrate the correlation among the different varying factors influencing the response coefficient (biodiesel conversion%). The perturbation plots, as shown in Fig. 12, are used to assess the mentoring consequence of one of the effective factors upon biodiesel conversion while retaining the other two parameters constant. Based on three axes, the most sensitive independent variable parameter upon the conversion of fabricated biodiesel is catalyst loading, which agrees with the ANOVA data (see Table 5), where the catalyst loading achieves a high *f*-value and the lowest possible *p*-value (<0.0001). This signifies that the catalyst loading substantially affects the response designs.

3.2.5. The 3D response surface diagram. The relationship among multiple variables that influenced the response parameter (biodiesel conversion%) is interpreted through RSM analysis. As shown in Fig. 13, 3D response surface diagrams are an effective method for indicating the interface and correlation among two various independent variables on the FAME conversion%, whereas the remaining independent variable remains constant.

Fig. 13a depicts a 3D response graph describing the influence of catalyst loading disparity and M : WCO on FAME conversion% while the time of the reaction is extended for 120 min. The FAME conversion rate is raised as the catalyst loading level is increased, as well as raising the M : WCO. Thus, increasing the catalyst amount accelerates the transesterification reaction by minimizing the activation energy and boosting the number of molecular collisions, resulting in more biodiesel conversion. As indicated in the ANOVA, catalyst loading (%) is the main influential factor in the methanolysis

Table 5 ANOVA for the polynomial design for biodiesel manufacture *via* transesterification methodology[a]

Source	Sum of squares	df	Mean square	*f*-Value	*p*-Value	
Model	366.93	9	40.77	53.13	<0.0001	Significant
A	209.35	1	209.35	272.81	<0.0001	
B	1.89	1	1.89	2.46	0.1478	
C	4.05	1	4.05	5.28	0.0444	
AB	4.95	1	4.95	6.44	0.0294	
AC	31.17	1	31.17	40.61	<0.0001	
BC	26.25	1	26.25	34.20	0.0002	
A^2	74.04	1	74.04	96.48	<0.0001	
B^2	8.09	1	8.09	10.54	0.0088	
C^2	2.91	1	2.91	3.79	0.0801	
Residual	7.67	10	0.7674			
Lack of fit	7.67	5	1.53			
Pure error	0.0000	5	0.0000			
Cor total	374.60	19				

[a] $R^2 = 0.9759$; standard deviation (SD) = 0.876; adjusted $R^2 = 0.9611$; coefficient of variation (C.V.%) = 0.9281%.

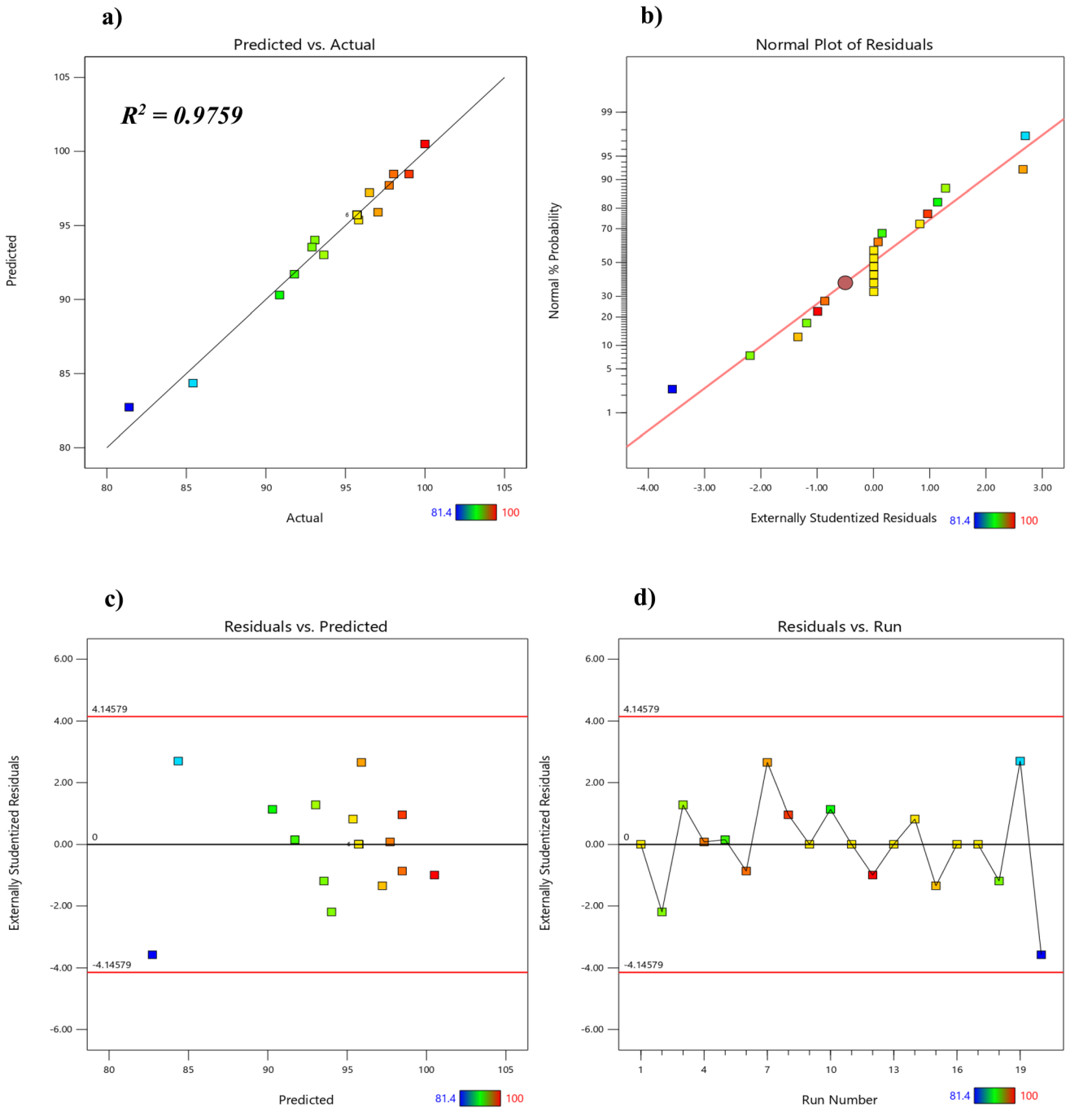

Fig. 11 RSM response diagrams results; (a) plot of experimentally verified (actual) biodiesel (FAME) conversion (symbol) *vs.* anticipated biodiesel conversion (straight line), (b) plot of standard percentage probability *vs.* residual biodiesel conversion, (c) plot of externally studentized residuals *vs.* response anticipated of biodiesel conversion, and (d) plot of externally studentized residual *vs.* experimental responses.

approach for FAME conversion, in contrast with the remaining factors (see Table 5). Furthermore, a catalyst loading of 3.5% and M : WCO of 7 : 1 yields the greatest feasible FAME conversion.

The corresponding surface graph in Fig. 13b reveals the disparity of FAME conversion% with the variation of catalyst amount and reaction time keeping the M : WCO with a constant value of 6 : 1. The noticeable improvement in FAME conversion with rising catalyst loading levels varying from 2.6 to 3.6% and reaction time is within the range from 84.3 to 120 min. An excessive catalyst dosage reduces FAME conversion owing to inadequate distribution through the methanolysis reaction.[22] Moreover, extending the transesterification time above 137.8 min would neither enhance the desired biodiesel conversion rate nor be cost-effective.

Fig. 13c portrays the implications of M : WCO and time on FAME conversion% with constant catalyst loading of 3.5%. The 3D curve appears to be comparatively smooth level,

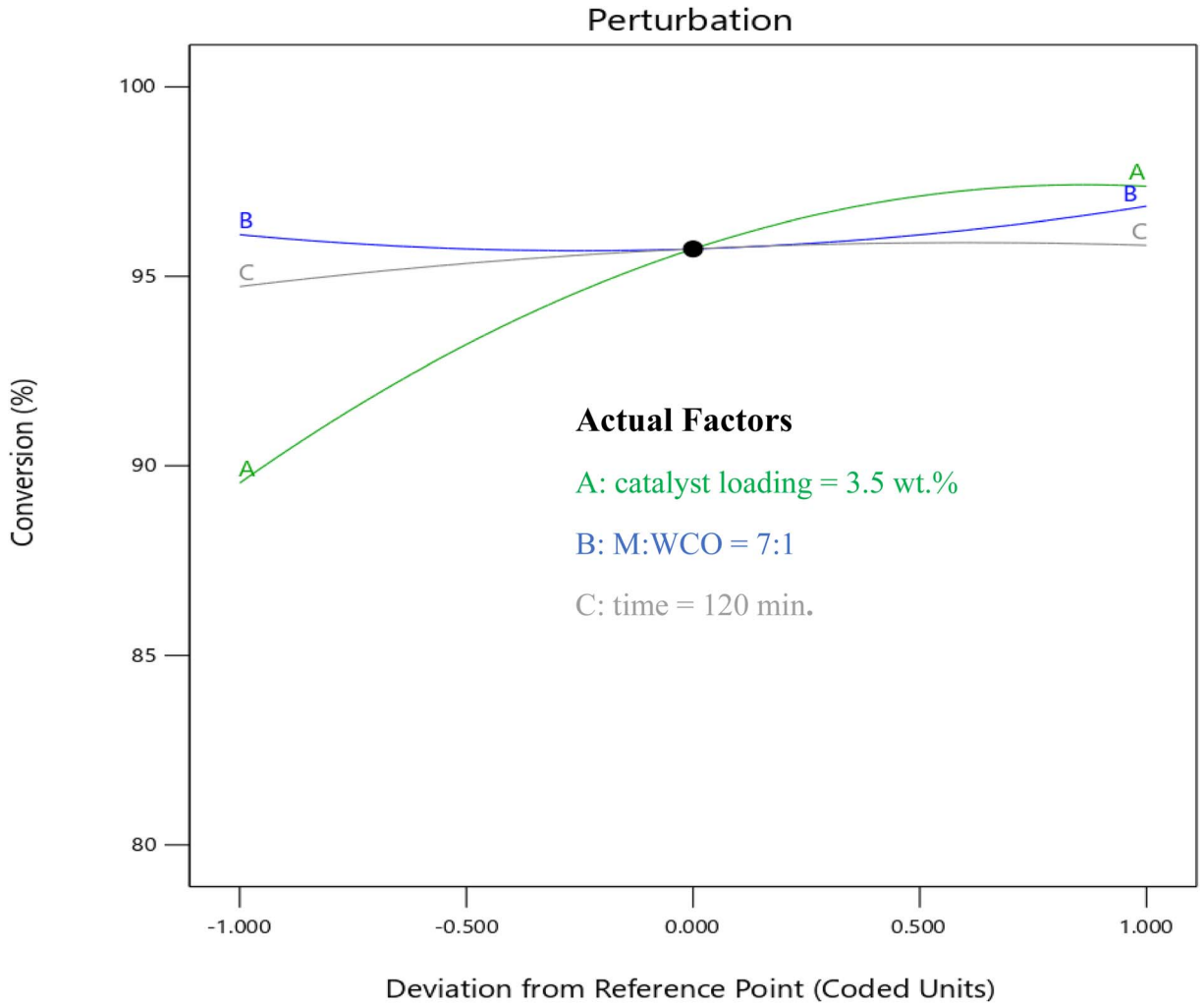

Fig. 12 Perturbation diagram for biodiesel conversion corresponding to the CCD for polynomial design (the experimental region's central instance: $A = 3.5$ wt%, $B = 7:1$, and $C = 120$ min).

implying that each of M : WCO and reaction time has minor effects on biodiesel conversion%, particularly with M : WCO and reaction time changes ranging from around 5.8 : 1 to 8 : 1 and 84 to 155 min, respectively. Where biodiesel conversion% shows no discernible variation. This is clarified by the ANOVA (see Table 5), since the M : WCO and time have a high *f*-value and *p*-value (>0.05), indicating that the M : WCO and reaction time are negligible to the FAME conversion produced *via* the methanolysis process compared with catalyst loading. As a result, the maximum biodiesel conversion rate necessitates low M : WCO and reaction time consumption as low as 7 : 1 and 120 min, respectively.

3.2.6. RSM numerical optimization methodology. Fig. 14 reveals the statistical optimization methodology to figure out the optimal condition of a particular methodology for producing biodiesel while reducing the independent variables to accomplish the maximum response of FAME conversion%. The desirability function is used to incorporate a competent process for determining the most viable reaction conditions. Several optimal conditions are achieved using RSM numerical optimization and the polynomial model (see eqn (5)). The desirability function of the proposed optimal conditions is around 0.763, with catalyst loading = 3.2 wt%, M : WCO = 5.8 : 1, and reaction time = 84.3 min at a consistent reaction temperature of 40 °C, producing an apical biodiesel conversion of 91.5%.

The transesterification reaction mechanism is predominantly associative, initiated by the nucleophilic attack of the methoxy anion on the electrophilic carbonyl carbon of the triglyceride molecule. This interaction forms a transient tetrahedral intermediate, which subsequently rearranges to release one molecule of methyl ester and a diglyceride. The reaction repeats through similar steps until all three glycerol-based ester bonds are cleaved, yielding three molecules of biodiesel (fatty acid methyl ester, FAME) and one molecule of glycerol as a byproduct, as demonstrated in Scheme 1.

3.3. Catalyst reusability

Catalytic durability and long-term activity are excellent indicators for a promising heterogeneous catalyst, particularly from an economic standpoint. In order to assess the reusability of the

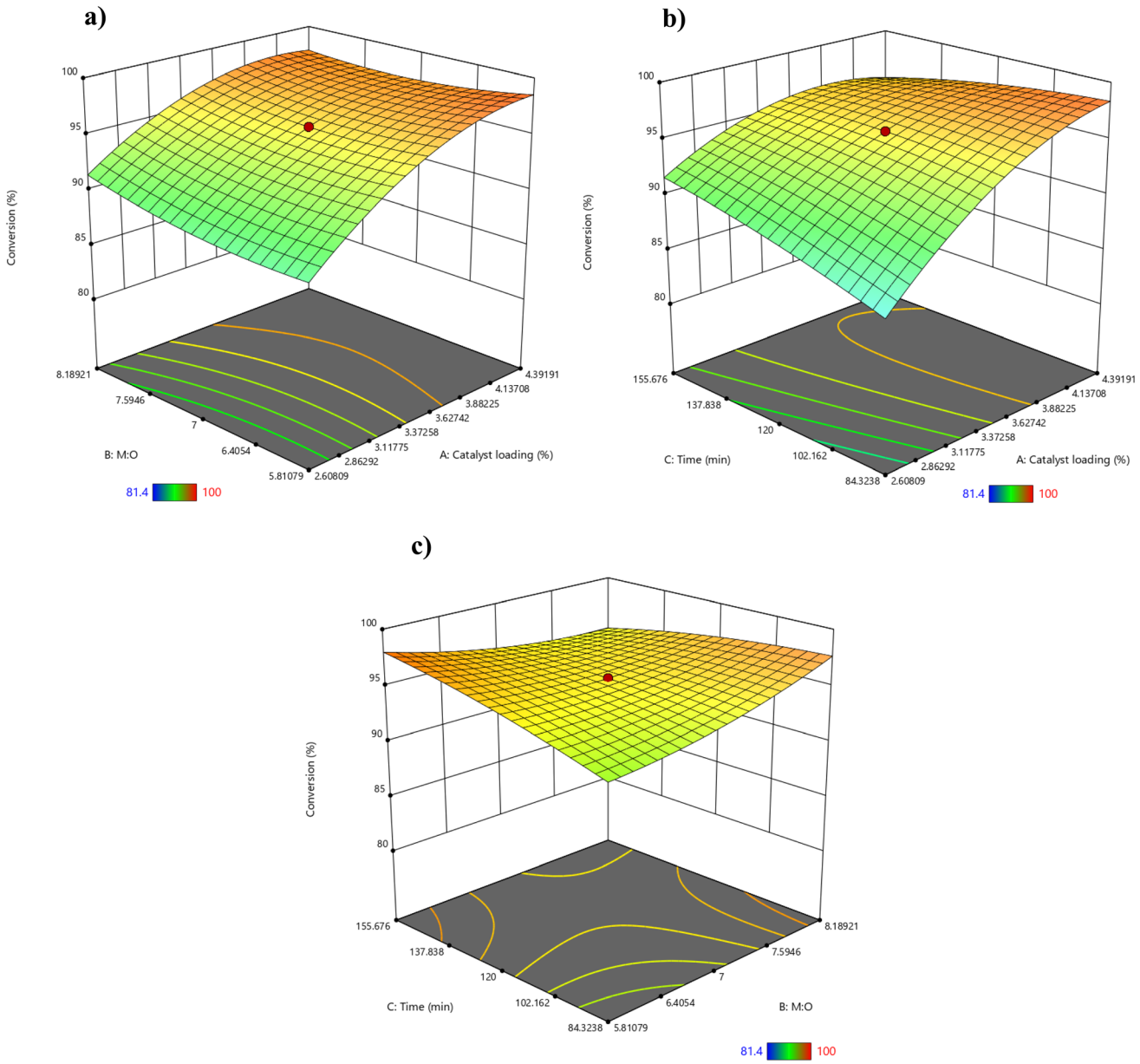

Fig. 13 3D surface diagrams depicting the effect of several binary factors on the FAME conversion (%); (a) catalyst loading and M : WCO, (b) catalyst loading and reaction time, and (c) M : WCO and reaction time.

proposed catalyst, it was centrifuged after the methanolysis reaction to extract it from the reaction matrix. The catalyst surface was rinsed with methanol and hot distilled H_2O to remove the adsorbed organic leftovers (glycerol, remaining oil, and biodiesel), and then it was dried at 80 °C. As a next step, the reactivated leftover catalyst was thermally activated for 3 h at 900 °C.[17] Therefore, thermal activation is required to retrieve the catalytic productivity for subsequent cycles. The retrieved catalyst was then subjected to additional runs at the previously found optimal conditions (3.2 wt%, 40 °C, 84.3 min, 5.8 : 1 M : WCO). As per Fig. 15, the CaO/K_2CO_3 catalyst maintains high catalytic efficacy for three consecutive cycles, with a small decline in FAME conversion to 91.1% in the second run and 82.6% in the third run. The 4th, and 5th runs show a significant drop in the catalytic performance. This is attributed to the leaching of the catalyst to the liquid phase in addition to the deactivation caused by the formation of calcium glyceroxide on the surface of the catalyst.[34] Furthermore, particle aggregation (*i.e.*, decrease in active surface area) is regarded as an additional cause for the reported decline in biodiesel conversion.[41]

3.4. Physicochemical characterization of the produced biodiesel fuel

The physical characteristics of the produced biodiesel fuel, including density at 15 °C, viscosity at 40 °C, pour point, cloud point, and flash point, have been established to guarantee the safe use of biodiesel in ignition engines. Density and viscosity are important characteristics of fuel atomizing and the

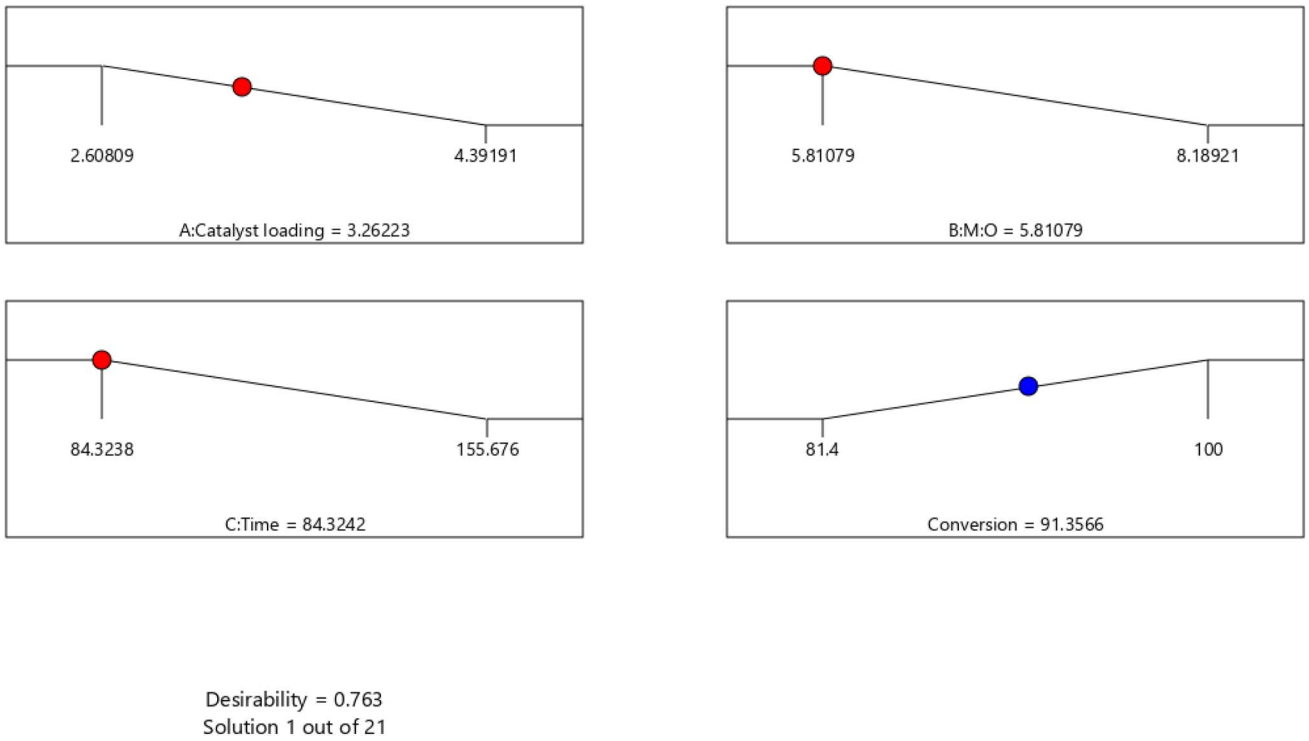

Fig. 14 RSM analysis for the numerical optimization methodology of biodiesel conversion (%).

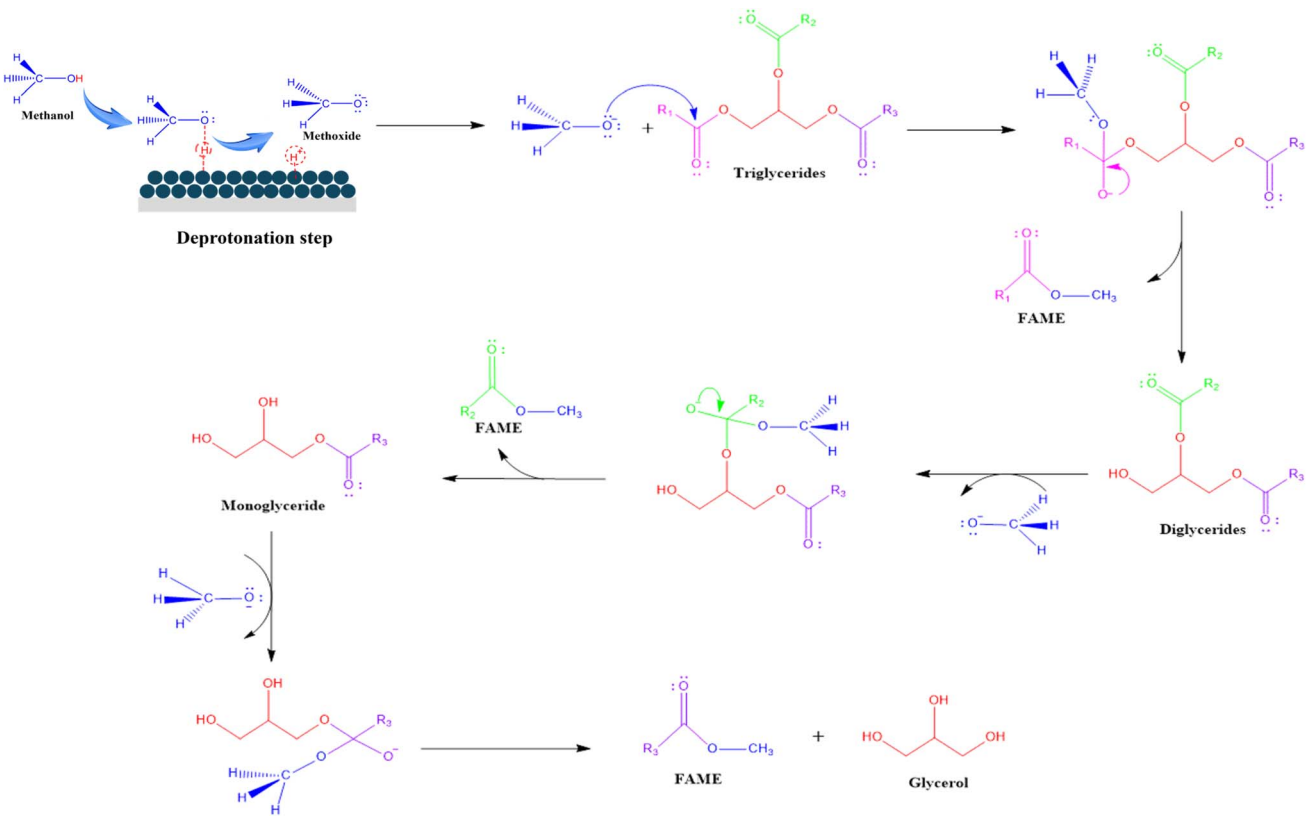

Scheme 1 Proposed mechanism of WCO transesterification to FAME using CaO/K_2CO_3 catalyst (represented by the black circles array at the top-left initial step) *via* methoxide ion formation and nucleophilic attack on triglycerides.

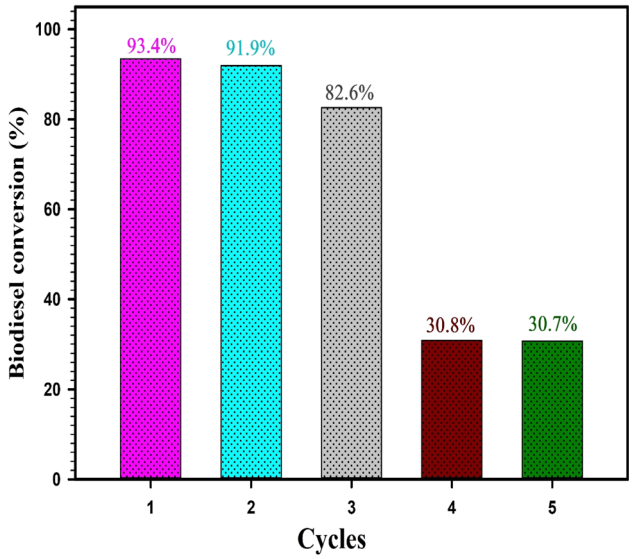

Fig. 15 Reusability investigation of CaO/K_2CO_3 nano-catalyst for five sequential transesterification cycles at the indicated optimum conditions of catalyst loading = 3.2%, M : WCO ratio 5.8 : 1, performed at 40 °C for 84.3 min.

productivity of combustion. Furthermore, the flash point determines the thermal resistance of biodiesel throughout transportation, along with its storage capacity. It also dictates the lowest possible temperature at which the fuel will explode on its own. Furthermore, cloud and pour points corroborate the biodiesel's cold-flow properties, which are beneficial for use in coldish environments. The quality of the obtained biodiesel fuel is determined according to the American Society for Testing and Materials (ASTM) methods, which are listed in Table 6. The results obtained are compared with the ASTM D-6751 and the European specification (EN-14214). The properties of the generated biodiesel are completely consistent with the biodiesel standards. This validates the good quality of the prepared biodiesel for efficient usage in a variety of environmental and climatic conditions.

3.5. Comparative study with similar systems

Table 7 compares the previously published findings in which CaO/K_2CO_3 has been applied as a nano-catalyst for biodiesel fabrication under optimal conditions with the present study. Bargole *et al.*[54] reported using marble refuse powder as a precursor of catalyst for biodiesel generation at optimum conditions; 6.8 wt% of catalyst loading at 64.8 °C for 180 min, with M : WCO of 15.9 : 1. In comparison to the present research, these parametric conditions take a long period and a large used quantity of methanol, raising the expense of producing biodiesel. Xie *et al.*[39] and Foroutan *et al.*[55] developed heterogeneous catalysts for biodiesel preparation at mild conditions, but at a time of 240 min and 200 min, respectively. This makes biodiesel manufacture a time-consuming process. Lukić *et al.*[56] succeeded in designing heterogeneous catalysts to overcome time-wasting through the biodiesel manufacturing process, but this success is reflected in employing a high reaction temperature of 120 °C, which is considered wasteful energy consumption and reflected in the expense of the overall method for biodiesel production. The current study has been successful in achieving a balance between reaction temperature and time consumption in the biodiesel manufacturing process *via* a methanolysis reaction. This is accomplished by employing K_2CO_3 as a support to CaO-based MWP as a nano-catalyst for making biodiesel below mild parametric conditions of 3.2 wt% catalyst loading with M : WCO of 5.8 : 1 at a low reaction temperature of 40 °C, which is near the room temperature, for a reaction time of only 84 min, achieving *ca.* 92% biodiesel conversion. Moreover, the primary environmental component of the current research is the worth of untreated WCO and MWP.

3.6. Economic feasibility study

Economic feasibility is a key driver in biodiesel production systems, which depend on the cost of input materials and the value of the final products.[22,60] The minimum selling price (MSP) of biodiesel can be estimated based on the costs of WCO, methanol, catalyst, and the value of glycerol as a by-product. As of 2025, the market price of WCO is approximately 0.52 USD per kg, which remains about one-third the cost of fresh vegetable oil. Methanol is priced at 0.38 USD per kg, while glycerol, depending on its purity, has a resale value ranging from 0.20 to 1.00 USD per kg. The catalyst used in this work is derived from MWP, an abundant and low-cost material, and is considered economically negligible in terms of input cost. Based on these parameters, the estimated MSP of biodiesel is ≤0.68 USD per kg under the current processing conditions. For comparison, Jae-Cheol Lee *et al.*[61] reported an MSP of 1.70 USD per kg for

Table 6 Biodiesel fuel physicochemical characterization in contrast to worldwide biodiesel standards (ASTM D-6751 and EN-14214)

		Limits		
Test	Test procedure	ASTM (D6751)[a]	EN (14214)[a]	FAME[b]
Density at 15.56 °C (g cm^{-3})	ASTM (D-4052)	—	0.86–0.90	0.883
Kinematic viscosity at 40 °C (mm^2 s^{-1})	ASTM (D-445)	1.9–6.0	3.5–5.0	3.9
Pour point (°C)	ASTM (D-97)	−15 to +16	—	0
Cloud point (°C)	ASTM (D-2500)	−3 to +12	—	6
Flash point (°C)	ASTM (D-92)	130 min	101 min	186

[a] Ref. 52 and 53. [b] FAME: biodiesel prepared through methanolysis of WCO (M : WCO of 5.8 : 1) at 40 °C for 84.3 min, and 3.2 wt% catalyst loading.

Table 7 Comparative survey of the acquired results and other comparable systems

		Catalyst preparation			Transesterification parameters					
Catalyst	Feedstock	Calcination (°C)	Time (h)	Catalyst loading (wt%)	Temp. (°C)	M : WCO	Time (min)	Reusable cycles[e]	Conversion (*C*)[c] or yield (*Y*)[d]	Ref.
CaO-based marble waste	WCO[a]	850	—	6.8	64.8	15.9 : 1	180	5	98.8 (*Y*)	54
CaO–$MgFe_2O_4$@K_2CO_3	UFO[b]	850	4	4	70	18 : 1	240	6	96.5 (*C*)	39
Biochar/CaO/K_2CO_3	Waste edible oil	500	3	4	65	18 : 1	200	9	98.8 (*C*)	55
35 wt% K_2CO_3/Al_2O_3	Sunflower	500	4	5	80	12 : 1	240	—	99.3 (*Y*)	57
40 wt% K_2CO_3/talc	Sunflower	550	4	4	65	6 : 1	240	5	98.4 (*Y*)	58
K_2CO_3/alumina/silica	Sunflower	600	—	2	120	15 : 1	15	1	93 (*Y*)	56
K_2CO_3/Al–Ca hydrotalcite	Soybean oil	550	5	2	65	13 : 1	120	4	87.4 (*Y*)	59
CaO/K_2CO_3	**WCO[a]**	**500**	**2**	**3.2**	**40**	**5.8 : 1**	**84.4**	**3**	**93.4 (*C*)**	**Current work**

[a] Waste cooking oil. [b] Used frying oil. [c] Evaluated by ^{1}H-NMR spectral analysis. [d] Evaluated by gas chromatography (GC analysis). [e] Number of runs before losing 50% of the catalyst activity.

WCO-based biodiesel, while Kalavathy Gengiah *et al.*[62] reported 0.84 USD per kg for biodiesel produced from *Codium tomentosum*. These comparisons indicate that the proposed catalyst and process are economically favorable and competitive with previously reported systems.

4. Conclusion

This work presented a sustainable strategy to overcome the limitations of K_2CO_3 as a catalyst for biodiesel production by supporting it on CaO derived from MWP. This incorporation significantly improved the catalyst's basicity, surface characteristics, and methanol activation capability, thereby enhancing the overall catalytic activity in the methanolysis of WCO to biodiesel. The synthesized CaO/K_2CO_3 nano-catalyst exhibited strong basic properties (as evident by the CO_2-TPD profile), accelerating hydrogen abstraction from methanol to create methoxide ions. The XRD pattern of the CaO/K_2CO_3, simultaneously with the BET assessment, confirmed the crystalline composition of the synthesized catalyst with a superior specific surface area. Additionally, the mesoporous structure, exceptional atomic framework, and extreme roughness of the nano-synthesized catalyst were elucidated by FE-SEM and HR-TEM analysis. The optimal calcination temperature was 500 °C, with a specific surface area of 1.53 $m^2\ g^{-1}$ and an average crystalline size of 14.6 nm, indicating nano-scale material synthesis and its superior catalytic efficacy. Employing response surface methodology, the optimal FAME conversion of approximately *ca.* 92% was obtained under mild conditions, *i.e.*, catalyst loading of 3.2%, at 40 °C for 84.3 min, and M : WCO of 5.8 : 1. The strong basicity of the CaO/K_2CO_3 nanocatalyst contributes to its effective catalytic performance in biodiesel production at relatively low temperatures. Catalytic stability tests indicate that the catalyst maintains a biodiesel conversion efficiency of over 85% across three consecutive reaction cycles. Furthermore, the physicochemical properties of the produced biodiesel comply with both ASTM (American) and EN (European) standards for fuel quality.

Conflicts of interest

There are no conflicts to declare.

Data availability

Should any raw data files be needed in another format, they are available from the corresponding author (Hosam H. Abdelhady, hosamhasan88@cu.edu.eg) upon reasonable request.

The authors declare that the data supporting the findings of this study are available within the paper and its SI. See DOI: https://doi.org/10.1039/d5ra04881h.

References

1 N. Anil, P. K. Rao, A. Sarkar, J. Kubavat, S. Vadivel, N. R. Manwar and B. Paul, Advancements in sustainable biodiesel production: A comprehensive review of bio-waste derived catalysts, *Energy Convers. Manage.*, 2024, **318**, 118884, DOI: 10.1016/J.ENCONMAN.2024.118884.

2 S. M. Hamed, A. F. Zedan, H. H. Abdelhady, N. M. Mohamed and A. M. Fekry, Graphitic carbon nitride/titania nanotube arrays for photoelectrochemical oxidation of methanol under visible light, *Int. J. Hydrogen Energy*, 2024, **90**, 918–930, DOI: 10.1016/J.IJHYDENE.2024.09.292.

3 A. A. Abdelraouf, A. M. Abdelrahim, M. G. Abd El-Moghny and M. S. El-Deab, Interface engineering: Enhancing the electrocatalytic activity of heterostructure NiFe-based alloy over valorized carbon waste towards water splitting, *Int. J.*

Hydrogen Energy, 2025, **101**, 556–567, DOI: 10.1016/J.IJHYDENE.2024.12.395.

4 A. A. Abdelraouf, A. M. Abdelrahim, M. G. Abd El-Moghny and M. S. El-Deab, Electrocatalysis by design: Enhanced bifunctional activity of exfoliated graphite rod modified with NiCo porous layers towards overall water splitting, *J. Environ. Chem. Eng.*, 2025, **13**(3), 117089, DOI: 10.1016/j.jece.2025.117089.

5 O. A. Mawlid, H. H. Abdelhady and M. S. El-Deab, Recent Advances in Magnetic Nanoparticle-Based Heterogeneous Catalysts for Efficient Biodiesel Production: A Review, *Energy Fuels*, 2024, **38**, 20169–20195, DOI: 10.1021/ACS.ENERGYFUELS.4C03555.

6 A. A. Meena R, M. J, R. Banu J, S. K. Bhatia, V. Kumar, G. Piechota and G. Kumar, A review on the pollution assessment of hazardous materials and the resultant biorefinery products in Palm oil mill effluent, *Environ. Pollut.*, 2023, **328**, 121525, DOI: 10.1016/J.ENVPOL.2023.121525.

7 A. M. Abdelrahim, M. G. A. El-Moghny, H. H. Abdelhady, H. S. Wali, M. M. Gamil, S. R. Fahmy, T. M. Abdel-Hamid, G. K. Mohammed, Y. A. Ahmed and M. S. El-Deab, Tailoring a facile electronic and ionic pathway to boost the storage performance of Fe_3O_4 nanowires as negative electrode for supercapacitor application, *Sci. Rep.*, 2024, **14**, 1–14, DOI: 10.1038/S41598-024-66480-5.

8 A. M. Ahmed, A. M. Abdelrahim, M. G. Abd El-Moghny, H. H. Abdelhady, N. M. A. Elhakiem, M. S. Shehate, N. W. Mohamed, S. R. Abdelrahman and M. S. El-Deab, Tuning heterostructured interface of binary hydroxide/metallic CoNi over Fe_3O_4 at modified graphite felt for enhanced oxygen evolution reaction, *Surf. Interfaces*, 2025, **72**, 107423, DOI: 10.1016/j.surfin.2025.107423.

9 M. Ahmed, K. A. Ahmad, D. V. N. Vo, M. Yusuf, A. Haq, A. Abdullah, M. Aslam, D. S. Patle, Z. Ahmad, E. Ahmad and M. Athar, Recent trends in sustainable biodiesel production using heterogeneous nanocatalysts: Function of supports, promoters, synthesis techniques, reaction mechanism, and kinetics and thermodynamic studies, *Energy Convers. Manage.*, 2023, **280**, 116821, DOI: 10.1016/J.ENCONMAN.2023.116821.

10 K. K. Jaiswal, S. Dutta, I. Banerjee, K. S. Jaiswal, N. Renuka, S. K. Ratha and A. K. Jaiswal, Valorization of fish processing industry waste for biodiesel production: Opportunities, challenges, and technological perspectives, *Renewable Energy*, 2024, **220**, 119601, DOI: 10.1016/J.RENENE.2023.119601.

11 S. Ghavami, F. Akhlaghian, S. Mohammadiazar and F. Rahmani, Biodiesel production from sunflower and waste cooking oils using K_2O/RGO catalyst, *Environ. Prog. Sustainable Energy*, 2024, **43**, e14235, DOI: 10.1002/EP.14235.

12 I. W. Khan, A. Naeem, M. Farooq, Z. A. Ghazi, T. Saeed, F. Perveen and T. Malik, Biodiesel production by valorizing waste non-edible wild olive oil using heterogeneous base catalyst: Process optimization and cost estimation, *Fuel*, 2022, **320**, 123828, DOI: 10.1016/J.FUEL.2022.123828.

13 M. Helmi, K. Tahvildari, A. Hemmati, P. A. Azar and A. Safekordi, Converting waste cooking oil into biodiesel using phosphomolybdic acid/clinoptilolite as an innovative green catalyst via electrolysis procedure; optimization by response surface methodology (RSM), *Fuel Process. Technol.*, 2022, **225**, 107062, DOI: 10.1016/j.fuproc.2021.107062.

14 A. Buasri, J. Kamsuwan, J. Dokput, P. Buakaeo, P. Horthong and V. Loryuenyong, Green synthesis of metal oxides (CaO-K_2O) catalyst using golden apple snail shell and cultivated banana peel for production of biofuel from non-edible Jatropha Curcas oil (JCO) via a central composite design (CCD), *J. Saudi Chem. Soc.*, 2024, **28**, 101836, DOI: 10.1016/j.jscs.2024.101836.

15 I. W. Sutapa, P. Taba, K. Shiomori, M. I. Taipabu and A. Kamari, Impregnation process and kinetics studies of MgO nanocatalyst/montmorillonite-K10 for biodiesel production from Cerbera odollam oil in modified-microwave reactor, *Kuwait J. Sci.*, 2024, **51**, 100209, DOI: 10.1016/J.KJS.2024.100209.

16 P. Andreo-Martínez, V. M. Ortiz-Martínez, M. J. Salar-García, J. M. Veiga-del-Baño, A. Chica and J. Quesada-Medina, Waste animal fats as feedstock for biodiesel production using non-catalytic supercritical alcohol transesterification: A perspective by the PRISMA methodology, *Energy Sustainable Dev.*, 2022, **69**, 150–163, DOI: 10.1016/J.ESD.2022.06.004.

17 O. A. Mawlid, H. H. Abdelhady and M. S. El-Deab, Boosted biodiesel production from waste cooking oil using novel $SrO/MgFe_2O_4$ magnetic nanocatalyst at low temperature: Optimization process, *Energy Convers. Manage.*, 2022, **273**, 116435, DOI: 10.1016/j.enconman.2022.116435.

18 M. R. Rizk, M. G. A. El-Moghny and M. S. El-Deab, 3D Macroporous Catalysts: Impact of Additives on the Morphology and Performance of Cu/Cu_2O Foam Prepared by Dynamic Hydrogen Bubble Template Towards Glycerol Electro-Oxidation, *J. Electrochem. Soc.*, 2020, **167**, 114505, DOI: 10.1149/1945-7111/ABA1A9.

19 M. R. Rizk and M. G. Abd El-Moghny, Controlled galvanic decoration boosting catalysis: Enhanced glycerol electro-oxidation at Cu/Ni modified macroporous films, *Int. J. Hydrogen Energy*, 2021, **46**, 645–655, DOI: 10.1016/J.IJHYDENE.2020.10.004.

20 M. R. Rizk, M. G. Abd El-Moghny and M. S. El-Deab, 3D Macroporous Catalysts: Impact of Additives on the Morphology and Performance of Cu/Cu2O Foam Prepared by Dynamic Hydrogen Bubble Template towards Glycerol Electro-Oxidation, *J. Electrochem. Soc.*, 2020, **167**(11), 114505, DOI: 10.1149/1945-7111/aba1a9.

21 M. R. Rizk, M. G. Abd El-Moghny, A. Mazhar, M. S. El-Deab and B. E. El-Anadouli, Dual-functioning porous catalysts: robust electro-oxidation of small organic molecules and water electrolysis using bimetallic Ni/Cu foams, *Sustainable Energy Fuels*, 2021, **5**, 986–994, DOI: 10.1039/D0SE01835J.

22 A. H. Abu-Ghazala, H. H. Abdelhady, A. A. Mazhar and M. S. El-Deab, Valorization of hazard waste: Efficient utilization of white brick waste powder in the catalytic

production of biodiesel from waste cooking oil via RSM optimization process, *Renewable Energy*, 2022, **200**, 1120–1133, DOI: 10.1016/J.RENENE.2022.10.045.

23 V. Loryuenyong, S. Rohing, P. Singhanam, H. Kamkang and A. Buasri, Artificial Neural Network and Response Surface Methodology for Predicting and Maximizing Biodiesel Production from Waste Oil with KI/CaO/Al_2O_3 Catalyst in a Fixed Bed Reactor, *ChemPlusChem*, 2024, **89**, e202400117, DOI: 10.1002/cplu.202400117.

24 Z. Al-Hamamre, A. Sandouqa, B. Al-Saida, R. A. Shawabkeh and M. Alnaief, Biodiesel production from waste cooking oil using heterogeneous KNO_3/Oil shale ash catalyst, *Renewable Energy*, 2023, **211**, 470–483, DOI: 10.1016/J.RENENE.2023.05.025.

25 D. Xiao, X. Li, Y. Zhang and F. Wang, Efficient Expression of Candida antarctica Lipase B in Pichia pastoris and Its Application in Biodiesel Production, *Appl. Biochem. Biotechnol.*, 2023, **195**, 5933–5949, DOI: 10.1007/S12010-023-04374-4/METRICS.

26 N. N. Ramlee, R. Md Illias, S. Toemen, R. A. Rahman, R. Selvasembian, W. Fatriasari, N. F. Ghazali and N. I. Wan Azelee, Co-immobilization of magnesium precursor and Candida rugosa lipase on alumina via covalent bonding for biodiesel production, *Fuel*, 2024, **377**, 132774, DOI: 10.1016/J.FUEL.2024.132774.

27 M. Ali Ijaz Malik, S. Zeeshan, M. Khubaib, A. Ikram, F. Hussain, H. Yassin and A. Qazi, A review of major trends, opportunities, and technical challenges in biodiesel production from waste sources, *Energy Convers. Manage.: X*, 2024, **23**, 100675, DOI: 10.1016/J.ECMX.2024.100675.

28 E. Sathiyamoorthi, J. Lee, M. D. Ramesh, R. M, D. Sandhanasamy, N. D. Nguyen and R. Shanmuganathan, Biodiesel production from eggshells derived bio-nano CaO catalyst – Microemulsion fuel blends for up-gradation of biodiesel, *Environ. Res.*, 2024, **260**, 119626, DOI: 10.1016/J.ENVRES.2024.119626.

29 E. Sathiyamoorthi, J. Lee, M. F. Albeshr, M. D. Ramesh, R. M and K. Brindhadevi, Effect of solar powered MgO/graphene nano catalysed biodiesel production from Scomber scombrus, *Environ. Res.*, 2024, **258**, 119407, DOI: 10.1016/J.ENVRES.2024.119407.

30 A. A. Fadairo, P. K. Wong, W. F. Ip, M. A. Ghadikolaei, Z. Cai, K. W. Ng and Z. D. Lian, Impact of neem oil biodiesel blends on physical and chemical properties of particulate matter emitted from diesel engines, *Environ. Pollut.*, 2024, **362**, 124972, DOI: 10.1016/J.ENVPOL.2024.124972.

31 R. A. Eldine, H. H. Abdelhady, S. A. Elhafez and M. S. El-Deab, Synthesis & Characterization of Novel CaO-based Heterogeneous Catalysts for Efficient Biodiesel Production from Waste Cooking Oil, *Egypt. J. Chem.*, 2024, **67**, 13–28, DOI: 10.21608/EJCHEM.2024.246023.8807.

32 N. C. Joshi, P. Gururani, P. Bhatnagar, V. Kumar and M. S. Vlaskin, Advances in Metal Oxide-based Nanocatalysts for Biodiesel Production: A Review, *ChemBioEng Rev.*, 2023, **10**, 258–271, DOI: 10.1002/CBEN.202200019.

33 Y. K. Venkatesh, M. P. Ravikumar, S. Ramu, C. H. Ravikumar, S. Mohan and R. Geetha Balakrishna, Developments in Titanium-Based Alkali and Alkaline Earth Metal Oxide Catalysts for Sustainable Biodiesel Production: A Review, *Chem. Rec.*, 2023, **23**, e202300277, DOI: 10.1002/TCR.202300277.

34 H. H. Abdelhady, H. A. Elazab, E. M. Ewais, M. Saber and M. S. El-Deab, Efficient catalytic production of biodiesel using nano-sized sugar beet agro-industrial waste, *Fuel*, 2020, **261**, 116481, DOI: 10.1016/J.FUEL.2019.116481.

35 M. Rahmayanti, I. Fatimah, A. Yahdiyani Ikhsani and D. Nur Azizah, The potential of calcium oxide nanocatalyst from chicken eggshells for biodiesel production using chicken fat waste, *Inorg. Chem. Commun.*, 2024, **165**, 112604, DOI: 10.1016/J.INOCHE.2024.112604.

36 S. P. Ahmed, S. Kataky, R. Dutta, A. J. Thakur and S. K. Dolui, Utilization of waste from paper industry as a heterogeneous base catalyst for the synthesis of biodiesel, *Environ. Prog. Sustainable Energy*, 2024, e14497, DOI: 10.1002/EP.14497.

37 R. Foroutan, S. Jamaleddin and R. Mohammadi, Application of walnut shell ash/ZnO/K_2CO_3 as a new composite catalyst for biodiesel generation from Moringa oleifera oil, *Fuel*, 2022, **311**, 122624, DOI: 10.1016/j.fuel.2021.122624.

38 O. A. Mawlid, H. H. Abdelhady and M. S. El-Deab, Highly active novel K_2CO_3 supported on $MgFe_2O_4$ magnetic nanocatalyst for low-temperature conversion of waste cooking oil to biodiesel: RSM optimization, kinetic, and thermodynamic studies, *J. Environ. Chem. Eng.*, 2023, **11**, 110623, DOI: 10.1016/J.JECE.2023.110623.

39 Y. Xie, D. Wang, S. F. Almojil, A. I. Almohana, A. F. Alali, Y. Zhou and A. Raise, CaO-$MgFe_2O_4$@K_2CO_3 as a novel and retrievable nanocatalyst for two-step transesterification of used frying oils to biodiesel, *Process Saf. Environ. Prot.*, 2023, **172**, 195–210, DOI: 10.1016/j.psep.2023.02.005.

40 R. Foroutan, S. J. Peighambardoust, R. Mohammadi, S. H. Peighambardoust and B. Ramavandi, Investigation of kinetics, thermodynamics, and environmental factors of biodiesel generation from sunflower and castor oil using rice husk ash/CuO/K_2CO_3 heterogeneous catalyst, *Environ. Technol. Innovation*, 2023, **32**, 103307, DOI: 10.1016/j.eti.2023.103307.

41 A. H. Abu-Ghazala, H. H. Abdelhady, A. A. Mazhar and M. S. El-Deab, Exceptional room temperature catalytic transesterification of waste cooking oil to biodiesel using environmentally-benign K_2CO_3/γ-Al_2O_3 nano-catalyst, *Chem. Eng. J.*, 2023, **474**, 145784, DOI: 10.1016/j.cej.2023.145784.

42 O. A. Mawlid, H. H. Abdelhady, M. G. Abd El-Moghny, A. Hamada, F. Abdelnaby, M. Kased, S. Al-Bajouri, R. A. Elbohy and M. S. El-Deab, Clean approach for catalytic biodiesel production from waste frying oil utilizing K_2CO_3/Orange peel derived hydrochar via RSM Optimization, *J. Cleaner Prod.*, 2024, **442**, 140947, DOI: 10.1016/J.JCLEPRO.2024.140947.

43 S. Ao, S. P. Gouda, M. Selvaraj, R. Boddula, N. Al-Qahtani, S. Mohan and S. L. Rokhum, Active sites engineered biomass-carbon as a catalyst for biodiesel production:

Process optimization using RSM and life cycle assessment, *Energy Convers. Manage.*, 2024, **300**, 117956, DOI: 10.1016/J.ENCONMAN.2023.117956.

44 B. Maleki and S. S. Ashraf Talesh, Sustainable biodiesel production from wild oak (Quercus brantii Lindl) oil as a novel and potential feedstock via highly efficient Co@CuO nanocatalyst: RSM optimization and CI engine assessment, *Renewable Energy*, 2024, **224**, 120127, DOI: 10.1016/J.RENENE.2024.120127.

45 A. H. Abu-Ghazala, H. H. Abdelhady, A. A. Mazhar and M. S. El-Deab, Enhanced low-temperature production of biodiesel from waste cooking oil: aluminum industrial waste as a precursor of efficient CaO/Al_2O_3 nano-catalyst, *Fuel*, 2023, **351**, 128897, DOI: 10.1016/J.FUEL.2023.128897.

46 M. Haghighi, L. B. Zare and M. Ghiasi, Biodiesel production from Spirulina algae oil over $[Cu(H_2PDC)(H_2O)_2]$ complex using transesterification reaction: Experimental study and DFT approach, *Chem. Eng. J.*, 2022, **430**, 132777, DOI: 10.1016/j.cej.2021.132777.

47 B. Ebadinezhad, M. Haghighi and H. Zeinalzadeh, Carbon-templated meso-design of nanostructured CeAPSO-34 for biodiesel production from free fatty acid and waste oil, *Renewable Energy*, 2022, **195**, 716–733, DOI: 10.1016/J.RENENE.2022.05.159.

48 E. Bekhradinassab, A. Tavakoli, M. Haghighi and M. Shabani, 2-Hydroxyethylammoniumsulfate ionic liquid performance as simultaneous fuel and sulfating agent in tablet-like manganese and iron incorporated titania synthesis: Biodiesel production from waste oil, *Fuel*, 2023, **340**, 127402, DOI: 10.1016/J.FUEL.2023.127402.

49 K. Saikia, A. Das, A. H. Sema, S. Basumatary, N. Shaemningwar Moyon, T. Mathimani and S. L. Rokhum, Response surface optimization, kinetics, thermodynamics, and life cycle cost analysis of biodiesel production from Jatropha curcas oil using biomass-based functional activated carbon catalyst, *Renewable Energy*, 2024, **229**, 120743, DOI: 10.1016/J.RENENE.2024.120743.

50 Q. Li, Y. Zhao, T. Liu, Z. Luo, K. Luo and T. Wang, Kinetic and optimization study of ultrasound-assisted biodiesel production from waste coconut scum oil using porous $CoFe_2O_4$@sulfonated graphene oxide magnetic nanocatalysts: CI engine approach, *Renewable Energy*, 2024, **236**, 121457, DOI: 10.1016/J.RENENE.2024.121457.

51 M. A. Abo El-Khair, M. El saied, A. O. Abo El Naga and A. S. Morshedy, Rapid and low-temperature biodiesel production from waste cooking oil: Kinetic and thermodynamic insights using a $KOH/ZnAl_2O_4$ nanocatalyst derived from waste aluminum foil, *Energy Convers. Manage.*, 2024, **318**, 118898, DOI: 10.1016/J.ENCONMAN.2024.118898.

52 A. S. Elgharbawy, A. I. Osman, A. G. M. El Demerdash, W. A. Sadik, M. A. Kasaby and S. E. Ali, Enhancing biodiesel production efficiency with industrial waste-derived catalysts: Techno-economic analysis of microwave and ultrasonic transesterification methods, *Energy Convers. Manage.*, 2024, **321**, 118945, DOI: 10.1016/J.ENCONMAN.2024.118945.

53 S. Kuepethkaew, S. Klomklao, N. Phonsatta, A. Panya, S. Benjakul and H. Kishimura, Utilization of Nile tilapia viscera oil and lipase as a novel and potential feedstock and catalyst for sustainable biodiesel production, *Renewable Energy*, 2024, **236**, 121514, DOI: 10.1016/J.RENENE.2024.121514.

54 S. S. Bargole, P. K. Singh, S. George and V. K. Saharan, Valorisation of low fatty acid content waste cooking oil into biodiesel through transesterification using a basic heterogeneous calcium-based catalyst, *Biomass Bioenergy*, 2021, **146**, 105984, DOI: 10.1016/J.BIOMBIOE.2021.105984.

55 R. Foroutan, R. Mohammadi, J. Razeghi and B. Ramavandi, Biodiesel production from edible oils using algal biochar/CaO/K_2CO_3 as a heterogeneous and recyclable catalyst, *Renewable Energy*, 2021, **168**, 1207–1216, DOI: 10.1016/J.RENENE.2020.12.094.

56 I. Lukić, J. Krstić, D. Jovanović and D. Skala, Alumina/silica supported K_2CO_3 as a catalyst for biodiesel synthesis from sunflower oil, *Bioresour. Technol.*, 2009, **100**, 4690–4696, DOI: 10.1016/J.BIORTECH.2009.04.057.

57 E. G. Silveira Junior, V. H. Perez, I. Reyero, A. Serrano-Lotina and O. R. Justo, Biodiesel production from heterogeneous catalysts based K_2CO_3 supported on extruded γ-Al_2O_3, *Fuel*, 2019, **241**, 311–318, DOI: 10.1016/J.FUEL.2018.12.074.

58 M. Z. Salmasi, M. Kazemeini and S. Sadjadi, Transesterification of sunflower oil to biodiesel fuel utilizing a novel K_2CO_3/Talc catalyst: Process optimizations and kinetics investigations, *Ind. Crops Prod.*, 2020, **156**, 112846, DOI: 10.1016/J.INDCROP.2020.112846.

59 C. Sun, F. Qiu, D. Yang and B. Ye, Preparation of biodiesel from soybean oil catalyzed by Al-Ca hydrotalcite loaded with K_2CO_3 as heterogeneous solid base catalyst, *Fuel Process. Technol.*, 2014, **126**, 383–391, DOI: 10.1016/j.fuproc.2014.05.021.

60 N. Rajendran, D. Kang, J. Han and B. Gurunathan, Process optimization, economic and environmental analysis of biodiesel production from food waste using a citrus fruit peel biochar catalyst, *J. Cleaner Prod.*, 2022, **365**, 132712, DOI: 10.1016/J.JCLEPRO.2022.132712.

61 J. C. Lee, B. Lee, Y. S. Ok and H. Lim, Preliminary techno-economic analysis of biodiesel production over solid-biochar, *Bioresour. Technol.*, 2020, **306**, 123086, DOI: 10.1016/J.BIORTECH.2020.123086.

62 K. Gengiah, B. Gurunathan, N. Rajendran and J. Han, Process evaluation and techno-economic analysis of biodiesel production from marine macroalgae Codium tomentosum, *Bioresour. Technol.*, 2022, **351**, 126969, DOI: 10.1016/J.BIORTECH.2022.126969.